CEAS Space Journal
https://doi.org/10.1007/s12567-026-00760-w

ORIGINAL PAPER

Reference datasets of primary rocket engine emissions for global launch inventories

Steffen Callsen[1] · **Moritz Herberhold**[1] · **Jascha Wilken**[1] · **Martin Sippel**[1]

Received: 8 April 2026 / Revised: 2 July 2026 / Accepted: 27 July 2026
© The Author(s) 2026

Abstract

Research on the radiative forcing and climate impact of emissions from the space transportation sector remains in its early stages. A critical component of advancing this field is the development of accurate global emission inventories, which depend fundamentally on the precise characterization of rocket engine exhaust products. One major current limitation is the reliance on simplified exhaust datasets that fail to capture the chemical and mass flow complexities introduced by different engine turbopump cycles. To address this gap, this study establishes a comprehensive new reference dataset of primary rocket engine emissions (modeled up to the nozzle exit plane). The dataset is anchored by a consistent 2200 kN thrust-class baseline, encompassing major cryogenic propellants, a hypergolic combination, and a solid rocket motor. For liquid propellant systems, both closed cycle (staged combustion) and open-cycle (gas generator) architectures are evaluated. Additionally, an exploratory methodology is introduced to assess the impacts of fuel film cooling by modeling a fraction of the total mass flow at a distinctly fuel-rich oxidizer-to-fuel ratio. Both the specific engine cycle and the implementation of film cooling are demonstrated to be critical factors in predicting black carbon exhaust fractions. Finally, these newly established reference datasets are compared against existing inventories. By employing 0D equilibrium combustion calculations at realistic oxidizer-to-fuel ratios and explicitly accounting for the distinct mass flows of different turbopump cycles, this study provides a highly consistent exhaust dataset to improve the fidelity of future atmospheric and climate models.

Keywords Rocket engine · Primary emissions · Global launch inventories · Staged combustion · Gas generator · Solid rocket motor

Abbreviations

Al	Atomic aluminum
AlH_2O_2Cl	Aluminum dihydroxide chloride
AlH_3O_3	Aluminum trihydroxide
Al_2O_3	Aluminum oxide
AlCl	Aluminum monochloride
$AlCl_2$	Aluminum dichloride
$AlCl_3$	Aluminum trichloride
AlOCl	Aluminum oxychloride
AlOH	Aluminum hydroxide radical
AlOHCl	Aluminum hydroxide chloride
$AlOHCl_2$	Aluminum hydroxide dichloride
C(gr)/BC	Carbon (solid, graphite), black carbon
C_2H_4	Ethylene
C_2H_6	Ethane
CH_2CO	Ketene
CH_3	Methyl radical
CH_3OH	Methanol
CH_4	Methane
Cl	Atomic chlorine
Cl_2	Molecular chlorine
CO	Carbon monoxide
CO_2	Carbon dioxide
COOH	Carboxyl radical
Fe_2O_3	Iron(III) oxide
$FeCl_3$	Iron(III) chloride
H	Atomic hydrogen
H_2	Molecular hydrogen
H_2O	Water
H_2O_2	Hydrogen peroxide
HCHO	Formaldehyde
HCN	Hydrogen cyanide
HCO	Formyl radical
HCOOH	Formic acid
HCl	Hydrogen chloride

✉ Steffen Callsen
Steffen.Callsen@dlr.de

[1] Institute of Space Systems, German Aerospace Center (DLR), Robert-Hooke-Straße 7, 28359 Bremen, Germany

Published online: 03 September 2026

$HClO_4$	Perchloric acid
HO_2	Hydroperoxyl radical
N_2	Molecular nitrogen
NH_3	Ammonia
NH_4ClO_4	Ammonium perchlorate
NO	Nitric oxide
O	Atomic oxygen
O_2	Molecular oxygen
OH	Hydroxyl radical

1 Introduction

With climate change being one of the defining challenges of the twenty-first century, understanding the atmospheric impacts of anthropogenic emissions is of critical importance. Over recent decades, extensive research has focused on emissions from major economic sectors, including electricity generation, heating, and transportation [1]. However, within the transportation sector, studies have largely focused on land-based, maritime, and aviation systems. Comparatively little effort has been dedicated to space transportation, particularly rocket launches. Moreover, investigations into the radiative forcing effects of aviation have primarily addressed emissions in the lower atmosphere, namely in the troposphere, tropopause, and lower stratosphere [2]. In contrast, rocket launches inject exhaust products throughout the entire atmospheric column, requiring the consideration of impacts across the stratosphere, mesosphere, and thermosphere.

Historically, generating reliable rocket emission inventories was not a high priority due to the assumption that the rocket exhaust is a small portion of the total anthropogenic emissions. However, this assumption has been challenged by initial results indicating that the specific effect (i.e., per kilogram emitted) of, e.g., black carbon (BC) emitted by launch vehicles could be orders of magnitude higher than equivalent emissions from ground or aviation sources [3].

In recent years, there has been growing activity in this area, including the publication of a number of launch emission specifications and/or inventories [4–9]. The inventories all face three principal challenges: the heterogeneity of launch vehicles, the lack of precise vertical profiles, and the uncertainties regarding the emitted species and particles. A detailed literature survey of the current state of these inventories and their rocket engine exhaust modeling is provided in chapter 2.

The German Aerospace Center (DLR) has launched the S3D-BETTER project to better characterize the life-cycle emissions of space systems, which includes establishing a detailed rocket emission inventory. This to be published database, the DLR Inventory of Global Emissions by Launchers (IGEL) [10], is designed as a year-by-year dataset to serve as input for atmospheric and climate models. Specifically, DLR-IGEL contains remodeled flight trajectories and their associated rocket engine emissions, targeting coverage of at least 95% of total global launch emissions.

The present study focuses on characterizing rocket engine exhaust products. Here, "exhaust" is defined as the combustion products up to the nozzle exit plane, equivalent to the term primary emissions. Downstream of the nozzle, near-field and far-field plume processes occur, during which the exhaust chemically and physically interacts with the surrounding atmosphere. Once plume temperature and velocity are in equilibrium with ambient conditions and only concentration gradients remain, the products are typically classified as "emissions" suitable for climate models. However, these post-nozzle processes are beyond the scope of this paper and will be addressed in future work. Any models assessing post-combustion still require the primary emissions as the initial state of the exhaust before evaluating the effects of mixing and dispersion.

The primary objective of this study is to establish a comprehensive set of reference engine exhaust datasets for varying propellant combinations and engine turbopump cycles to be used in future inventories. To achieve this, representative reference engines modeled within the DLR ENTRAIN project (European Next Reusable Ariane) serve as baseline cases. All ENTRAIN engines are sized for a common thrust level of 2200 kN, enabling a consistent comparison of exhaust compositions across different propellant combinations and turbopump cycles within an identical thrust class. The investigated liquid propellant combinations include liquid oxygen (LOX) paired with RP-1, liquid methane (LCH4), and liquid hydrogen (LH2). Critically, both staged combustion cycle and gas generator cycle engines are evaluated for each liquid propellant combination.

While the ENTRAIN project focused exclusively on cryogenic liquid propulsion, hypergolic engines and solid rocket motors (SRMs) remain vital components of the current civil launcher landscape. Therefore, new reference models for a staged combustion and a gas generator N2O4/UDMH engine, and an SRM have been created with a nominal thrust of 2200 kN to ensure consistency with the ENTRAIN engine class. Beyond SRMs and liquid rocket engines, hybrid propulsion systems are being developed and may achieve orbital capability in the future. While their distinct combustion characteristics will require novel exhaust reference profiles, the datasets presented here are designed to support current global orbital launch inventories, where hybrid engines do not yet play an operational role.

First, the current state of engine exhaust datasets used in launch vehicle emission inventories is summarized. Then the reference dataset is presented by comparing the nominal exhaust compositions across all investigated engines. Particular emphasis is placed on gas generator engines, where

the exhaust composition of the secondary gas generator flow differs substantially from that of the main thrust chamber. Second, an exploratory study assesses the exhaust impact of a potential fuel film cooling layer in the main combustion chamber. Finally, the newly established reference dataset is benchmarked against existing emission inventories.

2 Current state of global launch emission inventories

Generating accurate emission inventories for Earth System Models requires modeling a complex cascade of physical and chemical phases. This process extends from the internal dynamics of the engine to the eventual local dispersion of exhaust products. These phases can be categorized as follows:

- **Internal engine flow**: The main combustion chamber and supersonic expansion within the nozzle. Where applicable, this also includes secondary combustion flow streams.
- **Plume mixing/afterburning**: The near-field characterized by an inviscid supersonic core and the far-field where mixing with ambient air occurs across the entire plume cross-section, see Fig. 1. Significant secondary combustion takes place at altitudes with sufficient atmospheric density.
- **Atmospheric dispersion**: The diffusion of the cooled plume and subsequent non-linear chemical reactions happening on a mesoscale level, which is typically defined up to 1000 km, see Fig. 2

While final emissions must ultimately be quantified to assess their atmospheric impact, the focus of this paper is strictly on the first phase: accurately defining the primary emission source terms at the nozzle exit. In the rocket combustion chamber(s), fuel and oxidizer are ignited, and the resulting exhaust is accelerated to supersonic speeds in the nozzle. The chemical status at the nozzle exit represents the baseline primary emission "source term" for atmospheric modeling.

The final emissions needed for Earth system models can differ significantly from primary emissions due to the afterburning taking place during mixing with the local atmosphere. Even after the plume transitions from the near-field to the far-field, and mixes and cools completely, local concentrations of species and particles remain high. These spikes in concentration can drive non-linear chemical reactions over hours or days as the plume dilutes, altering the final products.

Secondary emissions generated during these phases include additional combustion byproducts resulting from the interaction between the plume and the atmosphere. Specifically, this involves the oxidation of unreacted species within the typically fuel-rich exhaust (afterburning) and the

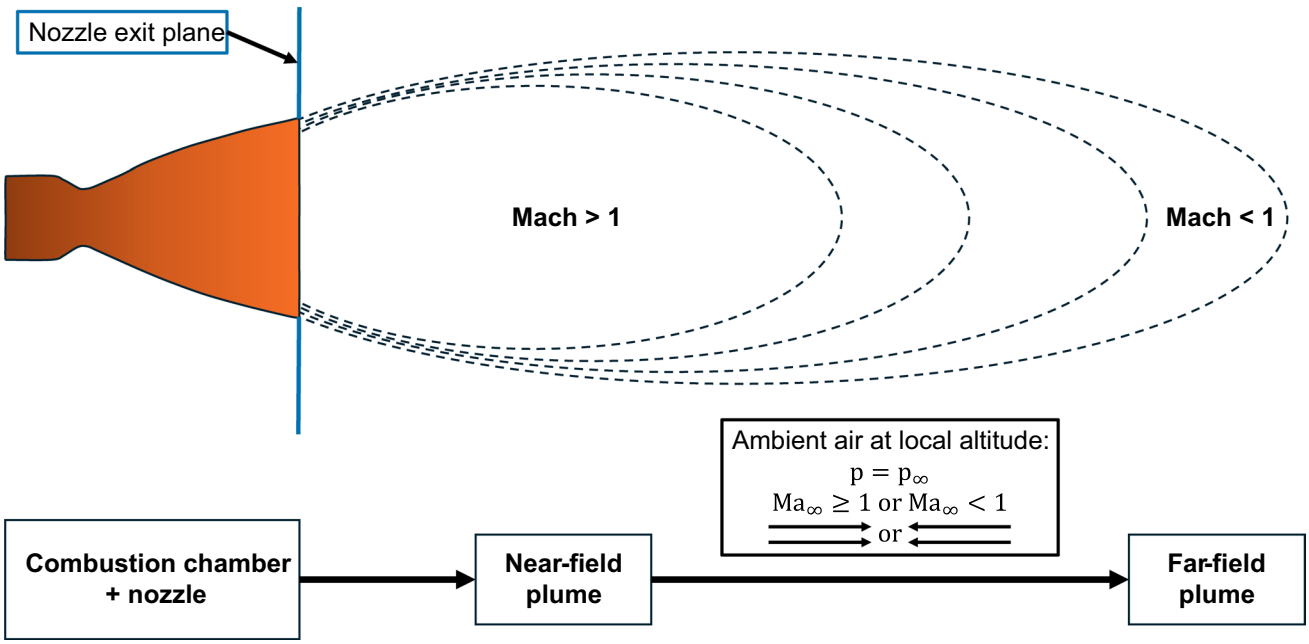

Fig. 1 Schematic illustration of the rocket engine exhaust including near-field and far-field plume. Arrows define the flow field direction which can be in plume direction (ascent) or against (descent)

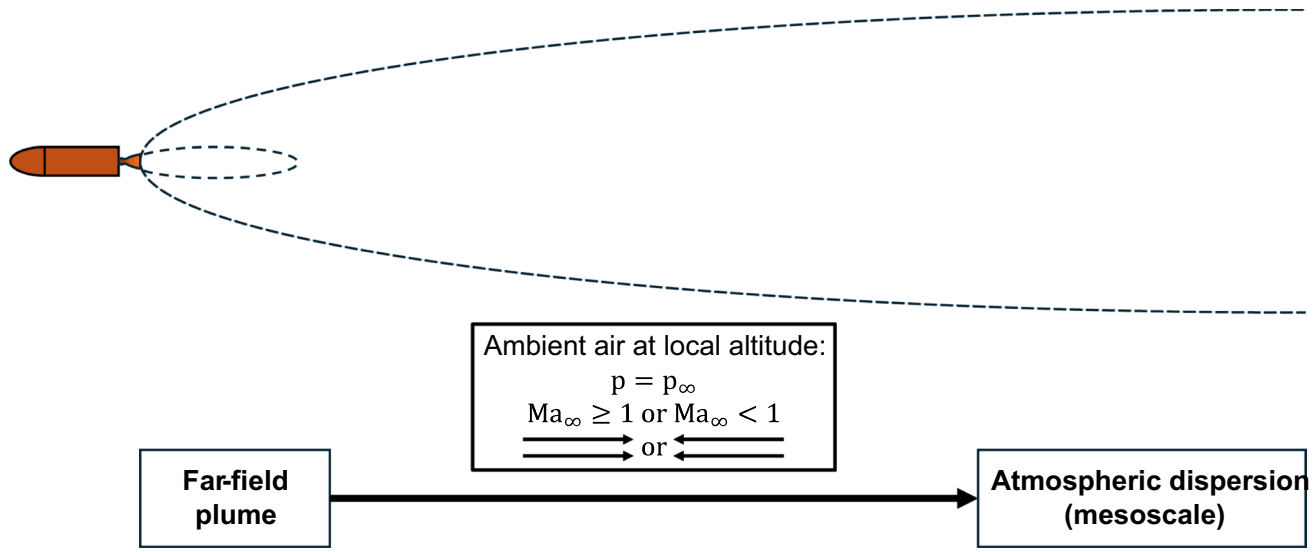

Fig. 2 Schematic illustration of the rocket engine exhaust including far-field plume and atmospheric dispersion on mesoscale level. Arrows define the flow field direction which can be in plume direction (ascent) or against (descent)

formation of compounds not present in the original propellants, such as thermally generated nitrogen oxides (NO_x).

Modeling this chain is challenging. It necessitates coupling highly heterogeneous fluid flow fields with complex chemistry, which are both sensitive to factors such as altitude, velocity, and engine orientation (e.g., for retro-propulsion burns) [17]. This difficulty is exacerbated by the diversity of launch hardware; active vehicles feature a wide range of propellants, engine cycles and nozzle configurations. Furthermore, the formation mechanisms of particulates, such as soot, remain poorly characterized under the fuel-rich conditions typical of rocket combustion.

Given these complexities, currently published exhaust inventories rely on significant simplifications. Many assume either zero or complete post-combustion and differentiate only by propellant type, ignoring the specific engine cycle.

Ross [4] adopts primary emission indices directly from propulsion literature, distinguishing only between major propellant groups. Pradon [5] appears to assume stoichiometric combustion. However, because rocket engines typically operate fuel-rich to maximize specific impulse and reap other launch-vehicle-related benefits, this assumption effectively implies complete afterburning with atmospheric oxygen, explaining derived values that exceed 1 kg/kg. While Barker [6] compiled primary emission indices from various literature sources and then applied post-combustion models, the sum of the primary indices given therein often exceeds 1 kg/kg as well. This discrepancy appears to stem from averaging emission indices for individual species across disparate literature sources, in some cases inadvertently mixing realistic fuel-rich engine models with theoretical complete stoichiometric combustion. Conversely, Brown [7] bases emission indices on the assumption of complete combustion (including the formation of thermal NOX), which implicitly requires atmospheric oxygen, yet applies them exclusively to the onboard propellant mass. Thus, this approach effectively ignores the mass of the consumed atmospheric air and underestimates the total emissions.

The Commercial Space Vehicle Emissions Modeling (CSVEM) document [8] offers a more comprehensive dataset. Here, specific engines are modeled using Chemical Equilibrium with Applications codes (discussed in section 3.2). This approach clearly defines primary emissions at the nozzle exit, models altitude-dependent post-combustion based on experimental data, and demonstrates sensitivity to the oxidizer-to-fuel ratio. Despite these advances, a critical gap remains: while reference engines are distinguished by propellant, the engine cycle itself is neglected. The models assume all propellants are processed through the main combustion chamber, which is a valid assumption for closed-cycle engines. However, for gas-generator cycle engines, a secondary flow has to be considered. This secondary flow is often extremely fuel rich and bypasses the main chamber, representing a distinct and unaccounted source of primary emissions.

The University of Stuttgart has published emission indices based on their Launch Emissions Assessment Tool (LEAT) [9]. The exhaust distributions are based on CEA plus an afterburning calculation and are listed in 5 km altitude intervals until an altitude of 120 km. As CEA does not output BC for a homogeneous combustion chamber distribution at typical oxidizer-to-fuel ratios, an approximation similar to CSVEM [8] seem to have been added. There are a number of instances, where the sum of the emissions

exceeds 1 by exactly the percentage of BC, indicating that BC has only been added to all other species. This is a slight inconsistency in the model. When comparing the inventories in Sect. 4.2, the LEAT output at an altitude of 120 km is used because there is no atmosphere left that can be applied to the post-combustion calculation. Thus, the distribution at 120 km can be assumed as primary emission indices.

LEAT is also recommended as basis in the 2025 European Space Agency's Space System Life Cycle Assessment Guidelines for space transportation [11]. However, the emissions spectrums provided in the guide are based on stoichiometric combustion and differ significantly from actual rocket engine exhaust distributions. The reasoning for this choice is not clearly understood. Additionally, it is not clear whether the emissions include post-combustion as the sum of the emission values is in some cases significantly over 1, in other cases not.

In summary, the current landscape of launch emission inventories is fragmented: models either oversimplify the engine's primary chemistry or introduce inconsistencies when combining primary emissions and afterburning models. This makes it unnecessarily challenging for the atmospheric modeling community to isolate true primary emission source terms and apply future afterburning and dispersion models. To address this gap and provide a reliable, standardized starting point for subsequent phases, the following section introduces a new reference dataset of primary emission indices derived from consistent thermodynamic and engine-cycle principles.

3 Reference dataset

In this chapter, the reference dataset is described. At first, the conceptualized rocket engines largely based on the ENTRAIN project are described. Additionally, newly added hypergolic engines and the solid rocket motor are also described. Second, the engine modeling process is described and validated with CEA as the established software. Third, the resulting reference engine exhaust profiles of the engines are described. Furthermore, an exploratory study investigating the effect of fuel film cooling is explained. At last, a local sensitivity study is performed to investigate the impact of key parameter variations on the exhaust profiles.

3.1 Generic rocket engines

ENTRAIN (European Next Reusable Ariane) was a large DLR study to systematically investigate different recovery methods in combination with propellant and engine cycle choices for two-stage-to-orbit launchers with a reusable first stage [12]. In this context, a number of generic engines of the 2200 kN class were sized to support this launcher study. While the designs were generic, their performance was validated with real engine data [13]. Because the first-stage engines are all designed for the same vacuum thrust of 2200 kN and with comparable engine cycle assumptions, they provide a solid foundation for a systematic comparison of the exhaust profile amid different engine cycles and propellant choices. Because the ENTRAIN project focused on reusability, it only investigated liquid propellant engines with liquid oxygen as oxidizer. The fuel was either RP-1, a highly refined kerosene, LCH4, or LH2. For each propellant combination, there is one closed-cycle engine and one open-cycle engine with a gas generator (GG).

However, solid rocket motors as well as hypergolic storable propellants still play a large role in launchers worldwide. For this reason, a solid rocket motor, a closed-cycle N2O4/UDMH engine, and a gas generator N2O4/UDMH engine are created additionally. Table 1 lists the most important model parameters for all engines in their nominal state. Compared to the cited study, the performance values are slightly different due to the usage of Rocket Propulsion Analysis (see Sect. 3.2) instead of the DLR program lrp2. The combustion chamber pressure of the GG engines is 12 MPa, and 16 MPa for the closed-cycle engines. While varying expansion area ratios were explored for the engines, this study focuses on 20 for the GG and 33 for the closed-cycle engines. The chosen turbopump configurations in the baseline study [13] follow typical engine designs and in case of the closed-cycle LOX/LH2 configuration, the DLR concept SLME. For the closed-cycle engines, the turbopump design has no impact on the exhaust profiles as all the propellants are combusted in the main combustion chamber.

The RP-1 and LCH4 engines only have one turbine that is connected via a single shaft to the oxidizer and fuel pumps. In the GG case, a small portion of fuel and oxidizer is separated from the main flow and burned in the gas generator, which then powers the turbine (see Fig. 3 left). To limit the temperature on the turbine blades, the combustion temperature is kept low by having a low O/F ratio. The exhaust is expelled via a separate nozzle.

The RP-1 and LCH4 closed-cycle versions are staged-combustion engines with an oxygen-rich pre-burner, further abbreviated as "oxygen-rich staged-combustion" (ORSC), where the whole oxygen is pre-burned with a small portion of the fuel at a very high O/F (see Fig. 3 right). The rest of the fuel is directly injected into the main combustion chamber (MCC) after being used for regenerative cooling. In this cycle, no propellant is expelled separately which increases performance significantly.

The LH2 engines have independent turbopumps for oxidizer and fuel, respectively. In the GG engine, a single gas generator produces the exhaust gas, which is then split to two turbines. The closed-cycle LH2 version is a full-flow staged-combustion engine (FFSC). Both the fuel and the

Table 1 Generic nominal engine parameters

Category	Parameters	Unit	LOX/ RP-1 ORSC	LOX/ RP-1 GG	LOX/ LCH4 ORSC	LOX/ LCH4 GG	LOX/ LH2 FFSC	LOX/ LH2 GG	N2O4/ UDMH ORSC	N2O4/ UDMH GG	Solid rocket motor
Main engine	Thrust, vacuum	kN	2203.0	2199.2	2200.0	2207.1	2200.0	2199.1	2200.0	2186.9	2200.0
	Thrust, sea level	kN	1941.0	1971.7	1941.5	1978.2	1942.3	1978.5	1936.9	1959.5	2008.4
	Isp, vacuum	s	334.8	309.5	349.3	325.6	435.6	410.1	319.0	302.2	270.0
	Isp, sea level	s	295.0	277.5	308.3	291.9	384.5	368.9	280.9	270.7	246.5
	Mixture ratio	–	2.6	2.23	3.25	2.72	6.0	6.03	2.67	2.35	2.098
	Total mass flow	kg/s	671.0	724.5	642.2	691.2	515.1	546.8	703.2	738.0	830.7
Thrust chamber and nozzle	Chamber pressure	MPa	16	12	16	12	16	12	16	12	10
	Mixture ratio		2.6	2.66	3.25	3.3	6.0	6.77	2.67	2.6	2.098
	Throat diameter	m	0.31	0.36	0.31	0.36	0.31	0.36	0.31	0.36	0.41
	Nozzle exit diameter	m	1.81	1.63	1.80	1.62	1.80	1.61	1.79	1.61	1.54
	Expansion area ratio	–	33	20	33	20	33	20	33	20	14
Gas generator	Combustion temperature	K		1100		780		780		1200	
	Mixture ratio	–		0.20		0.22		0.79		0.06	

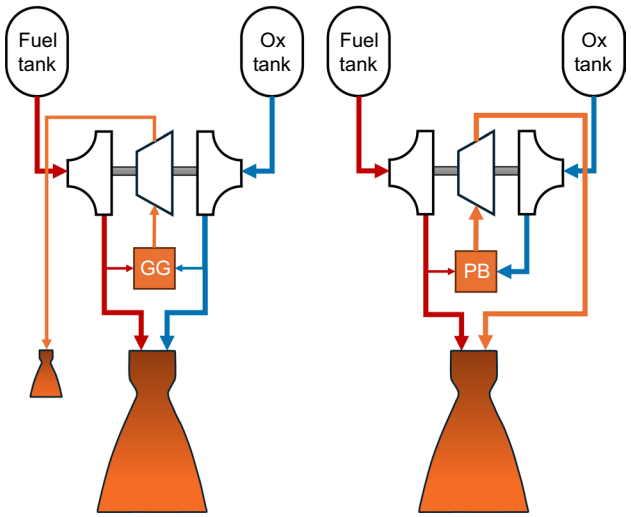

Fig. 3 Schematic flow diagrams of gas generator cycle (left) and staged combustion with oxygen-rich pre-burner cycle (right). Regenerative cooling flow is neglected in these diagrams

oxidizer are pre-burned with a small fraction of the other propellant and then power their own turbines.

Comparable to the LOX/RP-1 and LCH4 engines, the generic storable propellant engines also feature a single turbine connected to the oxidizer and fuel pump. The closed-cycle version is inspired by the RD-253/RD-275 family [14, 15], which power for example the Proton(-M) launcher, while the gas generator version is inspired by the RD-250 family [16] (Tsyklon-2 and Tsyklon-3 launchers).

The SRM is a typical modern P120C-like design with a composite propellant consisting of ammonium perchlorate (AP) as the oxidizer and aluminum as the fuel [17]. Hydroxyl-terminated polybutadiene (HTPB) is used as the binder, with iron oxide (Fe_2O_3) serving as a catalyst. The nominal propellant composition is based on Ref. [18], where the effect of iron oxide as a catalyst was tested with the involvement of the Italian solid rocket motor producer Avio. The nominal oxidizer-to-fuel ratio is 2.098, which means that 67.72% of the propellant is AP. The remaining fraction is the fuel with absolute shares of 18% aluminum, 14% HTPB, and 0.28% Fe_2O_3.

3.2 Engine modeling

The engines are modeled with the commercially available program Rocket Propulsion Analysis (RPA) [19, 20]. Equivalent to NASA's Chemical Equilibrium with Application (CEA) code [21], RPA determines performance and exhaust compositions through Gibbs free energy minimization assuming chemical equilibrium. However, it can also calculate the cycle performance which is critical for engines with an open gas generator cycle. There, a part of

the propellant is burned at a low oxidizer-to-fuel ratio to power the turbine. Afterwards, the gas is expelled through a separate nozzle. Because the exhaust of hydrocarbon-fueled GGs contains significant amounts of unburned hydrocarbons and soot, this modeling step is critical to establish a comprehensive reference dataset.

Because CEA is the accepted standard, a direct comparison of CEA and RPA is performed within this study in order to validate its equivalency specifically regarding the exhaust product composition. While the developers of RPA have published comparison data themselves [20], they focus primarily on performance characteristics and less on exhaust compositions.

The comparison is shown in Table 2 for LH2, LCH4, and RP-1 in combination with LOX. Given equivalent input settings, the exhaust product compositions are also almost equivalent. Only the CO_2 value for LOX/RP-1 is rounded differently on the 5th decimal place. The nozzle exit conditions also show small differences on the order of 0.1% or less, which is deemed acceptable for this study as it is far lower than other uncertainties.

In this study, the models for all methane-based engines assume pure liquid methane (LCH4). However, some operational engines may utilize liquid natural gas (LNG), which features small shares of additional hydrocarbons like ethane. Reference [13] suggests that LNG is viable as a rocket propellant provided that sulfur impurities are removed. From a thermochemical perspective, an increasing fraction of higher-order hydrocarbons increases the likelihood of BC precursor formation. However, ethane remains a low-molecular-weight hydrocarbon, which is significantly less prone to soot formation than the long-chain hydrocarbons and aromatics found in kerosene-based fuels like RP-1 [22]. Crucially, there is no standardized definition of aerospace-grade LNG composition similar to RP-1 [23, 24]. Therefore, to ensure consistency across our reference dataset, this study utilizes pure LCH4 in the modeling.

Table 2 Comparison of RPA and CEA for three propellant combinations

	LOX/LH2		LOX/LCH4		LOX/RP-1	
Parameter	RPA	CEA	RPA	CEA	RPA	CEA
Chamber pressure	6 MPa	60 bar	30 MPa	300 bar	12 MPa	120 bar
Mixture ratio	6.1	6.1	3.6	3.6	2.6	2.6
Oxidizer temperature	90 K	90 K	90 K	90 K	90 K	90 K
Fuel temperature	25 K	25 K	111.64 K	111.64 K	298 K	298 K
Contraction area ratio	2.5	2.5	2.5	2.5	2.1	2.1
Expansion area ratio	170	170	32	32	16	16
Nozzle flow assumption	Equilibrium	Equilibrium	Equilibrium	Equilibrium	Equilibrium	Equilibrium
Nozzle exit conditions						
Pressure	0.0019 MPa	0.01923 bar	0.1007 MPa	1.0074 bar	0.0899 MPa	0.8984 bar
Temperature	1007.11 K	1006.45 K	2056.80 K	2056.90 K	2146.68 K	2146.53 K
Mach number	5.2507	5.251	3.7398	3.740	3.3928	3.393
Effective exhaust velocity (vac)	4659.95 m/s	4658.9 m/s	3593.7 m/s	3593.6 m/s	3327.6 m/s	3327.7 m/s
Exhaust mass fractions						
Species	RPA	CEA	RPA	CEA	RPA	CEA
CO			0.09742	0.09742	0.29407	0.29407
CO2			0.44331	0.44331	0.41264	0.41265
H			0.00002	0.00002	0.00005	0.00005
H2	0.03259	0.03259	0.00367	0.00367	0.00702	0.00702
H2O	0.96741	0.96741	0.45493	0.45493	0.28562	0.28562
O						
O2			0.00005	0.00005	0.00002	0.00002
OH			0.00060	0.00060	0.00057	0.00057
Total	1.00000	1.00000	1.00000	1.00000	0.99999	1.00000

3.3 Engine exhaust profiles

In this chapter, the exhaust profiles of the reference engine configurations are presented as the baseline. Figure 4 displays the nominal exhaust profile of all investigated engines in stacked bar charts. The most relevant nominal engine exhaust species mass fractions are summarized in Table 3. All trace gases with mass fractions below 0.1% are summarized under the term "Other". The Appendices feature a table containing all trace gases and an acronym explanation of the chemical species.

First, the exhaust of the LOX/RP-1 engines consists predominantly of carbon monoxide (CO), carbon dioxide (CO_2), and water (H_2O), which together account for about 953 g/kg of the exhaust composition for the ORSC and 896 g/kg for the GG cycle. The contributions of these three species are relatively equal, with H_2O having a slightly lower fraction than CO and CO_2.

For ORSC, the remaining exhaust consists mainly of molecular hydrogen (H_2), atomic oxygen (O), molecular oxygen (O_2), and hydroxyl radical (OH), adding up to about 46 g/kg. The residual fraction is filled with different trace gases.

Because of the low O/F ratio of the gas generator, the LOX/RP-1 GG engine exhaust contains more species. Of the remaining 104 g/kg not accounted for by the dominant

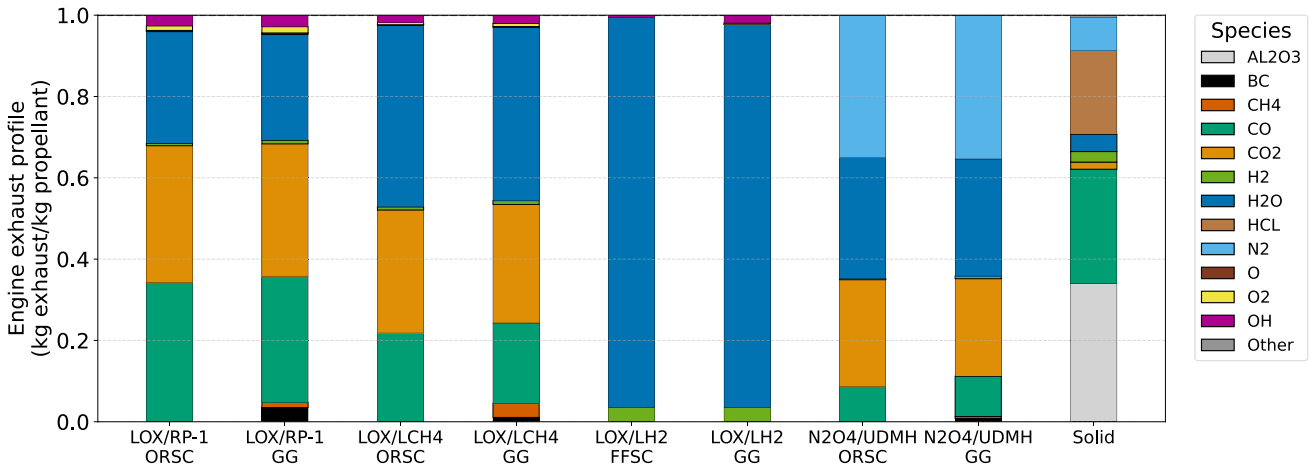

Fig. 4 Nominal engine exhaust profiles

Table 3 Summary of the most relevant engine exhaust species for all nominal engines

Species	Emission indices (g exhaust/kg propellant)								
	LOX/RP-1 ORSC	LOX/RP-1 GG	LOX/LCH4 ORSC	LOX/LCH4 GG	LOX/LH2 FFSC	LOX/LH2 GG	N2O4/UDMH ORSC	N2O4/UDMH GG	Solid rocket motor
Al_2O_3									339.7
BC		34.7		10.7				7.9	
CH_4		12.7		35.0				4.8	
CO	342.7	310.7	218.2	197.2			87.2	99.2	281.4
CO_2	336.1	325.4	302.6	291.5			262.1	239.8	17.5
$FeCl_3$									5.9
H_2	6.2	9.0	7.6	9.3	34.8	35.2	3.1	6.6	26.0
H_2O	274.5	260.2	447.0	426.7	959.4	941.9	297.7	287.9	42.5
HCl									205.7
N_2							348.4	352.7	80.7
O	2.9	3.7	1.1	1.4	0.1	0.7			
O_2	11.3	15.4	5.5	7.9	0.2	3.0	0.1	0.1	
OH	25.5	27.6	17.5	19.7	5.2	18.5	1.1	0.7	
Other	0.8	0.6	0.5	0.6	0.3	0.7	0.3	0.3	0.6

products, 34.7 g/kg is BC and 12.7 g/kg is methane (CH_4). The mass fraction of other minor, but relevant species, including H_2, OH, and O_2, is increased relative to the ORSC case. The sum of the trace gases stays at approximately the same level compared to the ORSC engine.

Second, the LOX/LCH4 engine exhaust also contains predominantly CO, CO_2, and H_2O, accounting 968 g/kg in total for the ORSC and 915 g/kg for the GG engine. However, in contrast to the approximately equal distribution in the LOX/RP-1 engines, H_2O has a far higher share at 447 and 427 g/kg, respectively. The remaining gases are distributed in a similar ratio compared to LOX/RP-1. The only major difference is a lower share of BC (10.7 g/kg) and a higher share of CH_4 (35 g/kg) for the GG engine.

Third, the bar charts of the LOX/LH2 engines look substantially different due to the absence of hydrocarbons in the fuel. Instead, water dominates the exhaust, accounting for approximately 959 and 942 g/kg, respectively. The GG exhaust differs from the FFSC configuration with higher shares of H_2, O, and OH.

Fourth, the exhaust of the N2O4/UDMH engines is dominated by molecular nitrogen (N_2) at about 350 g/kg, followed by H_2O at about 290 to 300 g/kg. While the closed-cycle engine has 262 g/kg CO_2 and 87 g/kg CO, the gas generator engine contains less CO_2 at about 240 g/kg and more CO at about 99 g/kg. Additionally, the GG engine has about 8 g/kg BC and 5 g/kg CH_4 resulting from the gas generator exhaust.

Finally, the exhaust profile of the solid rocket motor differs fundamentally from that of the liquid engines above. To interpret the resulting exhaust species, it is useful to first characterize the chemical composition of the propellant constituents. While the chemical compositions of aluminum (Al) and Fe_2O_3 are straightforward, ammonium perchlorate and hydroxyl-terminated polybutadiene require a more detailed description due to their molecular complexity. AP is formed from the reaction of ammonia (NH_3) and perchloric acid ($HClO_4$), yielding ammonium perchlorate (NH_4ClO_4). Therefore, it contains nitrogen, hydrogen, chlorine, and oxygen. HTPB consists of hydrocarbon polymer chains, terminated by hydroxyl functional groups. Consequently, it contains carbon, hydrogen, and oxygen.

The exhaust composition is dominated by aluminum oxide (Al_2O_3), which accounts for about 340 g/kg and results from the oxidation of aluminum during combustion. 281 g/kg of the exhaust mass is CO, while hydrogen chloride (HCl) represents about 206 g/kg. Nitrogen contributes approximately 81 g/kg to the exhaust. H_2O, H_2, and CO_2 account for about 43, 26, and 18 g/kg, respectively. Iron originating from the iron oxide additive reacts with chlorine to form iron trichloride ($FeCl_3$), contributing about 6 g/kg to the exhaust. The remaining combustion products are a large range of trace gases, which can be found in the Appendices.

Figure 5 shows the overall mass flow separated into the exhaust species in bar plots. The gas generator engines are additionally split into the main combustion chamber MCC and gas generator GG mass flow. While the engines with the hydrocarbon fuels require a GG mass flow of about 6–7%, this is only 3.6% for the LOX/LH2 engine. All these propellants are expelled at a low exhaust velocity, which thereby reduces the overall performance significantly. In this figure, all species with a share of less than 0.1% are summed up as "Other", which is barely visible in this diagram.

The analysis of the gas generator engines is further supported by Fig. 6 and complemented by Table 4, in which the stacked bar charts are separated into the exhaust originating from the main thrust chambers (left) and from the gas generators (right) for each propellant combination.

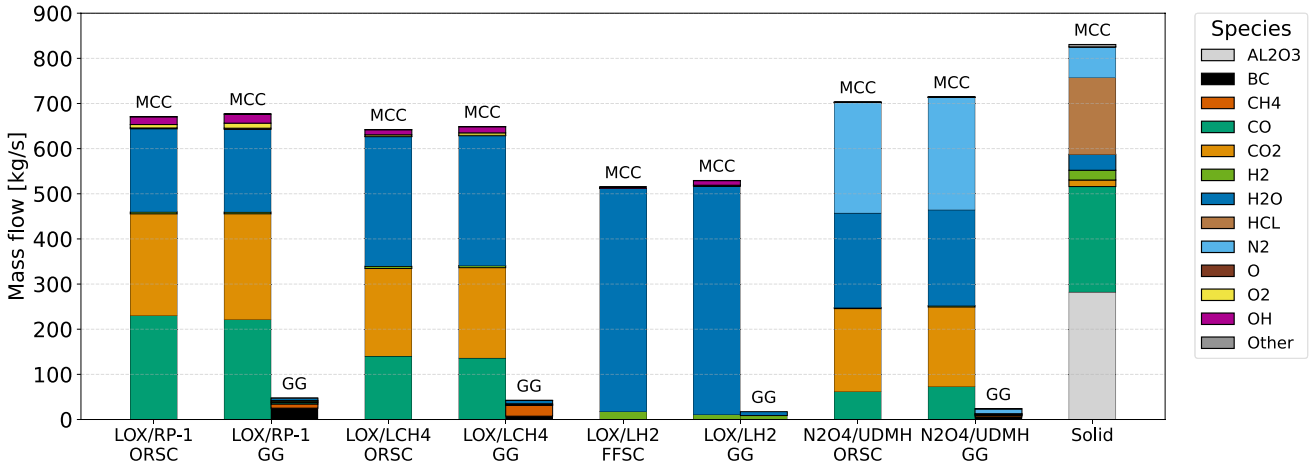

Fig. 5 Mass flow of all investigated engines showing the main chamber exhaust for all closed-cycle engines and a split of the main chamber and the GG exhaust for all GG engines

Table 4 Open-cycle engine exhaust profiles split into main combustion chamber and GG exhaust

Species	Emission indices (g exhaust/kg propellant)							
	LOX/RP-1 GG		LOX/LCH4 GG		LOX/LH2 GG		N2O4/UDMH GG	
	MCC	GG	MCC	GG	MCC	GG	MCC	GG
BC		529.5		174.1				247.3
CH_4		193.1		572.0				151.2
CO	327.9	65.7	209.5	8.8			101.3	35.8
CO_2	345.1	44.2	308.7	27.8			247.6	2.2
H_2	5.7	55.9	7.1	42.7	19.8	503.0	4.0	85.9
H_2O	270.6	111.6	443.2	174.6	956.5	497.0	296.8	20.9
N_2							349.3	456.2
O	4.0		1.5		0.7			
O_2	16.4		8.4		3.1		0.1	
OH	29.5		20.9		19.1		0.7	
Other	0.8	0.0	0.7	0.0	0.8	0.0	0.2	0.5

Because of the low mass flow rate of the GG exhaust, the charts representing the main thrust chambers closely resemble those of the total engine exhaust. In contrast, the exhaust compositions of the gas generators differ substantially. For the LOX/RP-1 GG, the exhaust is dominated by 530 g/kg BC, followed by 193 g/kg CH_4. The remaining fraction, roughly one quarter of the exhaust, is distributed among H_2O, H_2, CO_2, and CO and trace gases. In case of the LOX/LCH4 engine, the GG exhaust is mainly composed of CH_4, representing about 572 g/kg, while BC contributes only 174 g/kg. The remaining approximately 250 g/kg consist mainly of H_2O, with smaller fractions of H_2, CO_2, and CO. For the LOX/LH2 configuration, the GG exhaust is composed almost equally of H_2O and H_2. The GG exhaust of the hypergolic N2O4/UDMH engine is dominated by N_2 at about 456 g/kg, followed by BC (247 g/kg) and CH_4 (151 g/kg). The remaining 150 g/kg consist mainly of H_2, CO, and H_2O.

3.4 Exploratory film cooling study

Modeling the rocket engines with CEA or RPA assumes a spatially homogeneous O/F ratio in the combustion chamber. As a result, closed-cycle hydrocarbon engines with sufficiently high O/F ratios do not produce BC in the equilibrium exhaust. However, in reality, soot or BC formation is observed even in these engines because the mixture ratio is not homogenous. In particular, many engines use fuel film cooling (FC) at the chamber walls to reduce the combustion temperature and by that the thermal load on the regeneratively cooled structure. BC can be formed in these areas of low O/F ratios. Such spatial effects are not captured by 0D equilibrium models. While future studies shall look at this effect specifically by using two-dimensional kinetics tools like NASA's TDK [25], this study aims at exploring the film cooling effect by using an RPA surrogate model. However, it must be stressed that such a surrogate model comes with significant limitations. The real boundary layer effects are

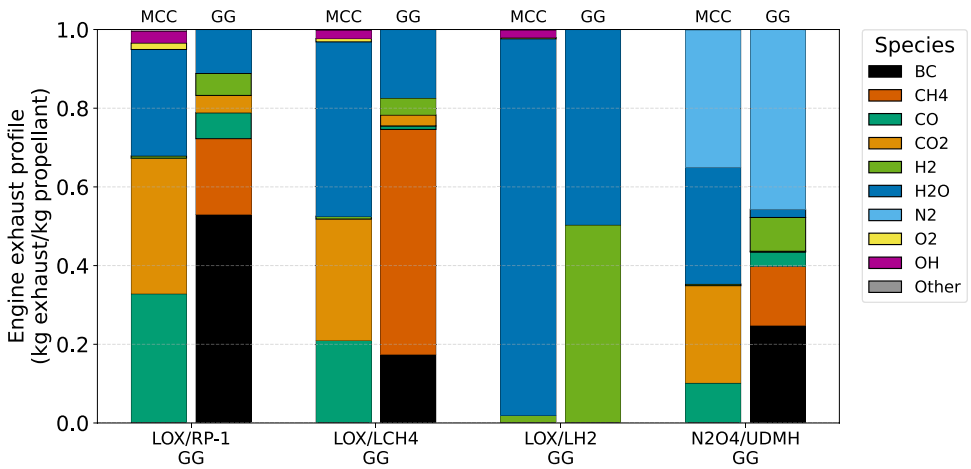

Fig. 6 Open-cycle engine exhaust profiles split into main combustion chamber and GG exhaust

Table 5 Exhaust profiles including film cooling

Species	Emission indices (g exhaust/kg propellant)			
	LOX/RP-1 ORSC FC	LOX/RP-1 GG FC	LOX/LCH4 ORSC FC	LOX/LCH4 GG FC
BC	8.0	42.3	0.6	11.4
CH_4	3.2	15.4	4.5	39.0
CO	344.1	312.5	223.8	202.8
CO_2	328.8	318.2	299.1	288.1
H_2	7.5	10.3	9.3	10.9
H_2O	269.2	255.3	438.9	419.2
O	2.8	3.6	1.0	1.4
O_2	10.9	14.9	5.3	7.6
OH	24.8	26.8	17.0	19.1
Other	0.7	0.7	0.5	0.5

extremely complicated and cannot be replicated with such a simplified engineering model. Nevertheless, the model is expected to be closer to reality than completely neglecting the effect.

Furthermore, spatial inhomogeneities inherent to real engines like imperfect propellant atomization and complex flow fields due to the injector plate design [26] are beyond the scope of 0D equilibrium modeling. In practice, these localized effects could act as an additional source of BC precursors in the exhaust.

For this exploratory study, the film cooling mass flow is assumed to come from the primary fuel flow and is injected into the main combustion chamber. It should be noted that in some gas generator engines, the low-pressure turbine exhaust gas is injected as film cooling into the nozzle (turbine exhaust gas injection) [27]. However, because the gas is injected into the divergent part of the nozzle at low pressures and temperatures, subsequent chemical reactions until the nozzle exit plane are limited by slow chemical reaction kinetics and insufficient mixing time. Consequently, it is assumed that the exhaust profiles at the nozzle exit plane of such engines would effectively be identical to the standard gas generator engine.

The surrogate model separates the main combustion chamber into the central chamber and the film cooling area, applying two separate equilibrium calculations. Based on the RD-0110 engine [28], 3 percent of the total chamber mass flow is assumed to have a low fuel-rich O/F ratio that shall resemble the film cooling. While equilibrium temperature will not be reached in such a fuel-rich environment, the real boundary layer temperature distribution will vary significantly with lower temperatures at the injection point of the pure fuel film and higher temperatures downstream. An O/F ratio of 0.6 for LOX/RP-1 and 1.1 for LOX/LCH4 is chosen keeping the equilibrium combustion chamber temperature below 1400 K, which is higher than the GG combustion temperature but still substantially below the central combustion chamber temperature. This provides an estimate for the species composition at the nozzle exit plane where the fuel film has partially combusted with the surrounding flow.

The results are shown in Fig. 7, complemented by Table 5. Because the film cooling effect is mainly of interest for engines with a hydrocarbon fuel, this exploratory study is only performed for LOX/RP-1 and LOX/LCH4. Compared to the nominal engines, the share of BC increases for all investigated engines, with the closed-cycle engines now having a share of BC for the first time.

The LOX/RP-1 ORSC engine has a BC fraction of 8 g/kg. Similarly, the BC share of the LOX/RP-1 GG engine is increased by 7.6 g/kg. In contrast, the film cooling for

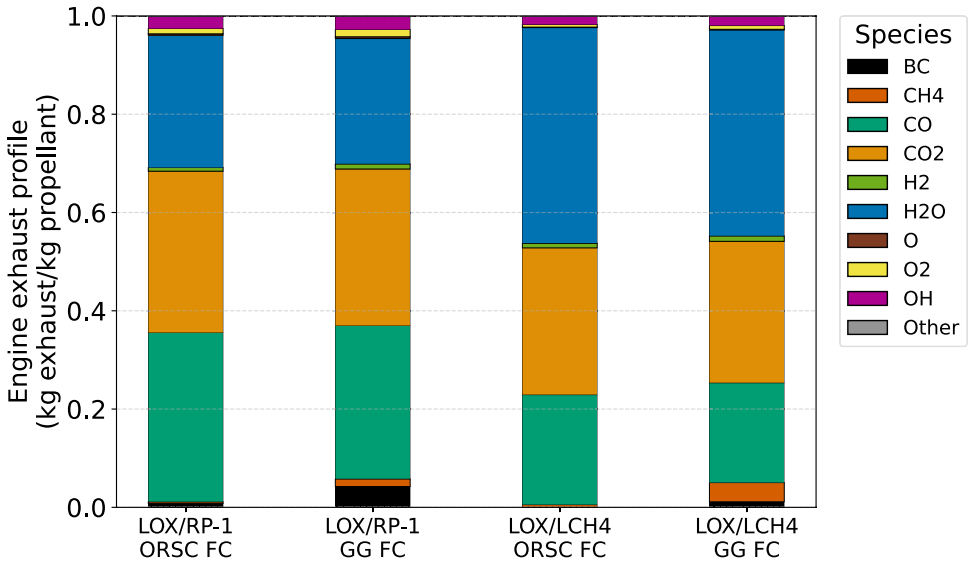

Fig. 7 Engine exhaust profiles including film cooling

the LOX/LCH4 engines creates substantially less BC, with only 0.6 g/kg for the closed-cycle engine, and an increase of 0.7 g/kg for the GG engine.

These results indicate that the film cooling exhaust may have a BC stake that cannot be neglected for the calculation of the overall exhaust. However, there is a large difference between the propellant combinations which is in agreement with observations from actual engine images.

3.5 Local sensitivity analysis

To assess the uncertainty of the reference dataset and constrain the effect of parameter variations, a local sensitivity analysis (LSA) is performed for specific parameters in the model that are expected to have a large impact on the overall species distribution. This includes the global O/F ratio, the frozen area ratio, the GG temperature, and the film cooling fraction.

3.5.1 Oxidizer-to-fuel ratio

The first variation parameter is the O/F ratio in the main combustion chamber. While engines typically have a nominal O/F ratio for optimal performance, they usually operate within an operational boundary that allows shifting the O/F ratio. In this analysis, the O/F is varied by ± 0.03, except for LOX/LH2 where it is increased to ± 0.05 due to the overall higher nominal O/F. Figures 8 and 9 show the LSA results for the closed-cycle and open-cycle engines, respectively. The figures are supplemented with Tables 6 and 7 giving the precise exhaust values for the variation cases.

For the hydrocarbon and hypergolic engines, a higher O/F ratio increases the CO_2 fraction and decreases the CO fraction of the exhaust. There is a slight decrease in H_2O for the hydrocarbon engines, while it increases slightly for the hypergolic engines. In case of the hydrogen engines, the H_2O levels increase slightly for the closed-cycle engine while it decreases for the open-cycle engine.

3.5.2 Frozen area ratio

In the reference datasets, shifting equilibrium is assumed in the main chamber nozzle until the flow is frozen at a distinct area ratio in the divergent part of the nozzle based on empirical recommendations [29], which are shown in Table 8. Because there is no data for LOX/LCH4, its value is assumed to be between LOX/RP-1 and LOX/LH2.

Due to the rapid decrease in temperature and pressure in this part of the nozzle, the uncertainty of this parameter is considered high. To assess this uncertainty, the exhaust species are shown for two additional cases, which display the extreme boundaries. First, freezing the flow directly at the throat. Second, maintaining shifting equilibrium until the nozzle exit plane. For the gas generator exhaust, the flow is always assumed to be frozen at the throat.

Figures 10 and 11 show the results for all propellant combinations for the closed-cycle and open-cycle engines, respectively. The specific data are listed in Tables 9 and 10, respectively.

3.5.3 Gas generator temperature

The gas generator combustion temperature is the RPA model input that defines the GG O/F ratio. Figure 12 and the listed values in Table 11 show a parametric variation of the GG temperature by 50 K in either direction. Because of cycle

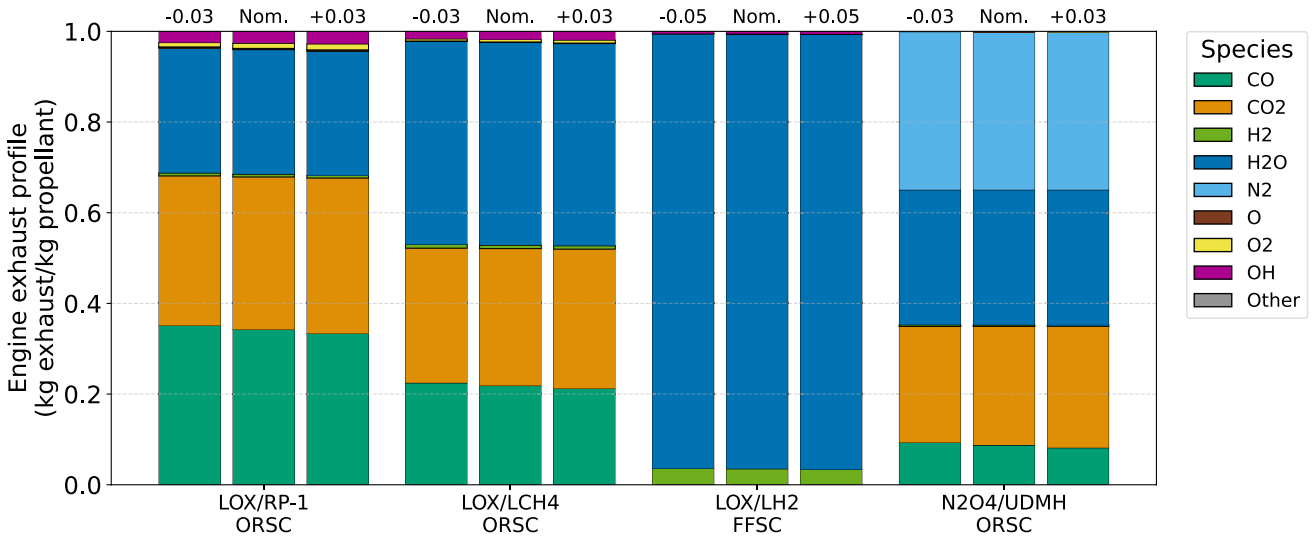

Fig. 8 LSA of closed-cycle engine exhaust profiles for O/F ratio variation

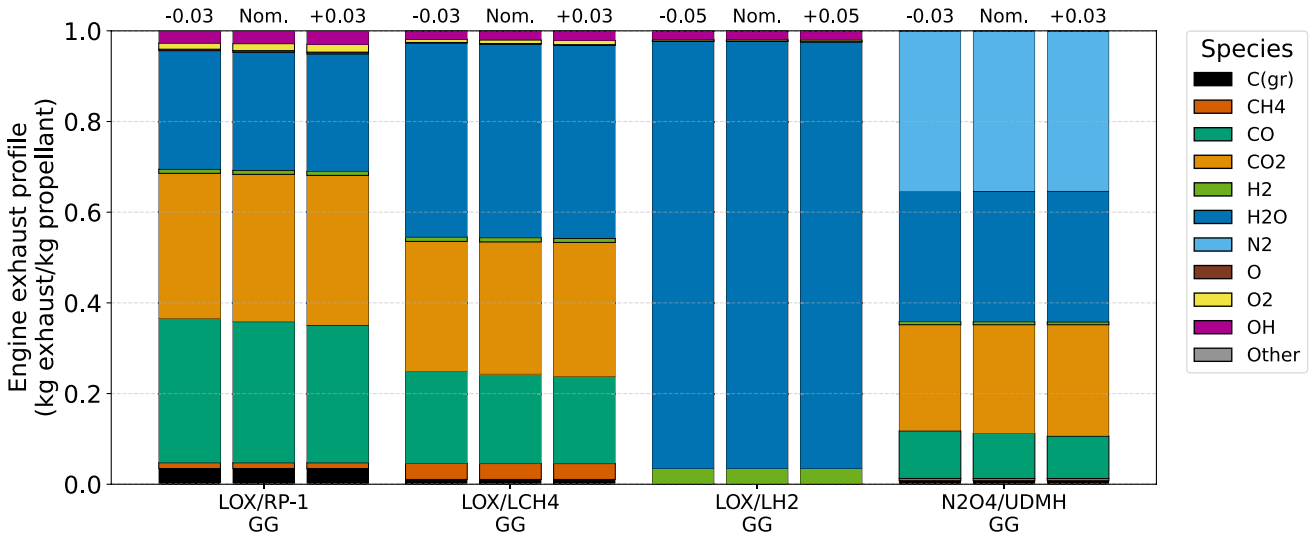

Fig. 9 LSA of open-cycle engine exhaust profiles for O/F ratio variation

Table 6 LSA results of closed-cycle engines for O/F ratio variation

Species	Emission indices (g exhaust/kg propellant)							
	LOX/RP-1 ORSC		LOX/LCH4 ORSC		LOX/LH2 FFSC		N2O4/UDMH ORSC	
	− 0.03	+0.03	− 0.03	+0.03	− 0.05	+0.05	− 0.03	+0.03
CO	351.6	334.1	224.4	212.2			93.2	81.2
CO_2	329.6	342.4	297.5	307.6			255.9	268.3
H_2	6.5	5.9	8.0	7.3	35.9	33.7	3.5	2.8
H_2O	275.4	273.6	447.9	445.9	958.8	960.0	297.5	297.8
N_2							348.8	348.0
O	2.6	3.2	0.9	1.2	0.1	0.1		
O_2	9.6	13.1	4.5	6.6	0.1	0.2	0.1	0.2
OH	24.0	26.9	16.2	18.8	4.7	5.7	0.8	1.3
Other	0.7	0.8	0.6	0.4	0.4	0.3	0.2	0.4

Table 7 LSA results of open-cycle engines for O/F ratio variation

Species	Emission indices (g exhaust/kg propellant)							
	LOX/RP-1 GG		LOX/LCH4 GG		LOX/LH2 GG		N2O4/UDMH GG	
	− 0.03	+0.03	− 0.03	+0.03	− 0.05	+0.05	− 0.03	+0.03
BC	34.8	34.7	10.7	10.6			7.9	7.9
CH4	12.7	12.6	35.1	34.9			4.9	4.8
CO	318.4	303.3	202.7	191.9			104.9	93.5
CO_2	319.9	330.5	287.1	295.8			234.1	245.6
H_2	9.2	8.7	9.6	9.0	35.2	34.4	7.0	6.2
H_2O	261.1	259.1	427.9	425.5	941.9	941.0	287.3	288.4
N_2							353.1	352.3
O	3.4	4.0	1.3	1.6	0.7	0.8		
O_2	13.4	17.4	6.7	9.2	3.0	3.5		
OH	26.3	28.8	18.5	20.8	18.5	19.6	0.6	0.9
Other	0.8	0.9	0.4	0.7	0.7	0.7	0.2	0.4

Table 8 Frozen area ratio for different propellant combinations [29]

Propellant combination	Frozen area ratio
LOX/RP-1	1.3
LOX/LCH4	1.8 (Assumption)
LOX/LH2	3.0
N2O4/UDMH	6.0

convergence issues in RPA, the lower boundary for the propellant combination N2O4/UDMH could only be moved by 10 K.

The results show that for all hydrocarbon and hypergolic engines, an increasing gas generator temperature (or a higher GG O/F ratio) leads to a lower share of BC and CH_4. For LOX/LH2, more H_2O and less H_2 is produced in the gas generator with a higher GG temperature leading to small changes in the overall distribution.

3.5.4 Film cooling

Because the propellant used for film cooling highly depends on the specific engine design and for example

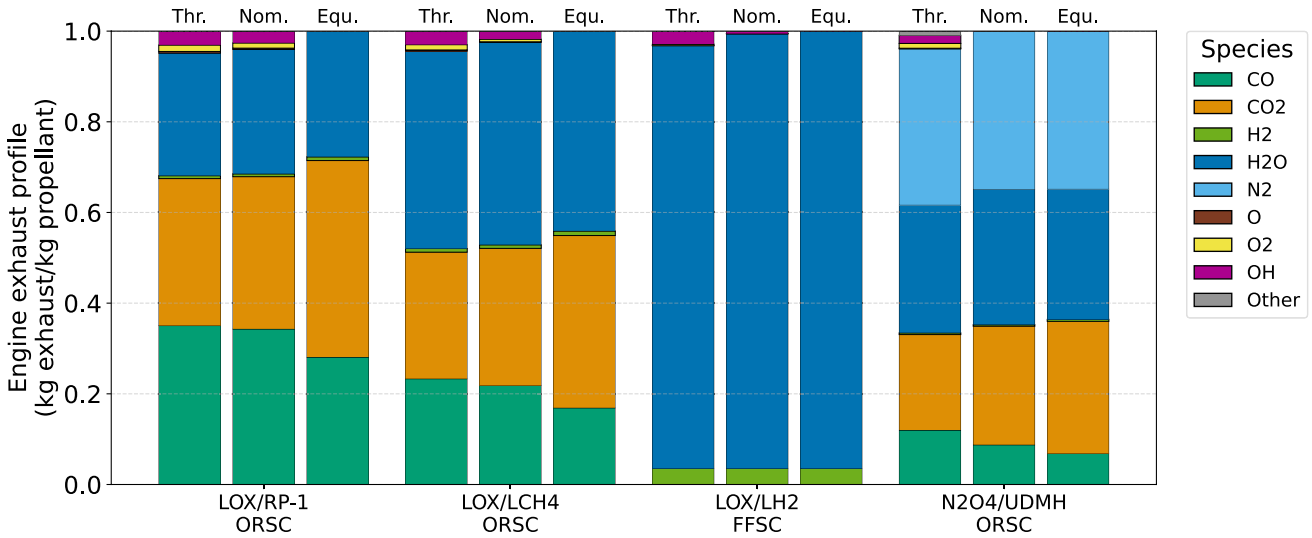

Fig. 10 LSA of closed-cycle engine exhaust profiles assuming frozen flow at the throat, nominal conditions, and shifting equilibrium to the nozzle exit plane

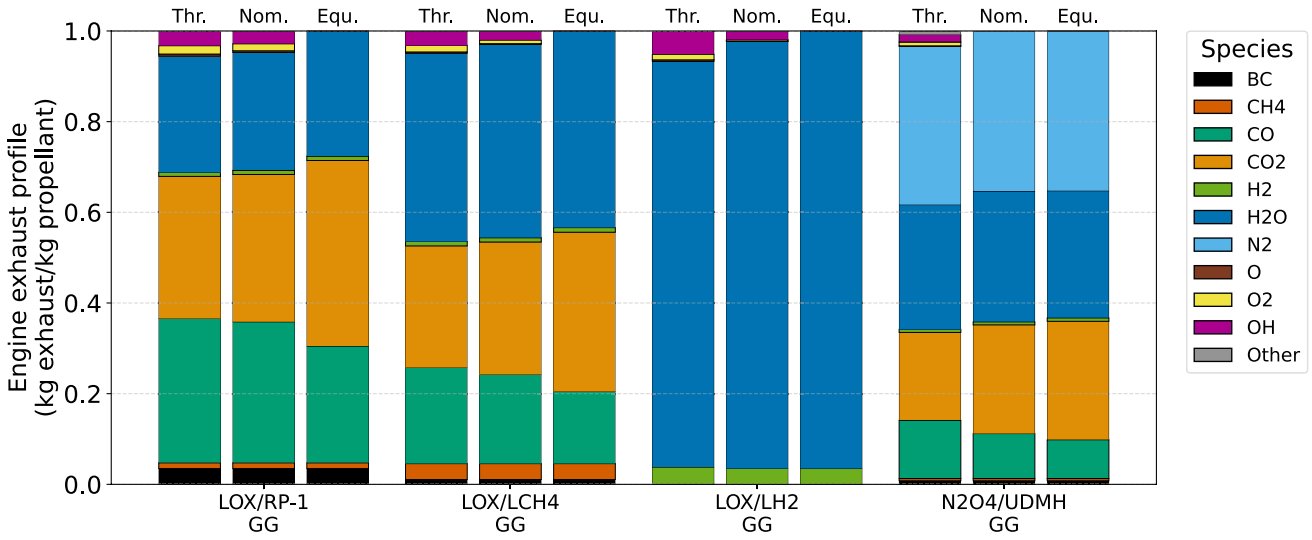

Fig. 11 LSA of open-cycle engine exhaust profiles assuming frozen flow at the throat, nominal conditions, and shifting equilibrium to the nozzle exit plane

Table 9 LSA results of closed-cycle engines assuming frozen flow at the throat and shifting equilibrium to the nozzle exit plane

Species	Emission indices (g exhaust/kg propellant)							
	LOX/RP-1 ORSC		LOX/LCH4 ORSC		LOX/LH2 FFSC		N2O4/UDMH ORSC	
	Throat	Equil	Throat	Equil	Throat	Equil	Throat	Equil
CO	350.0	280.5	232.9	168.7			119.8	68.7
CO_2	324.7	434.0	279.6	380.4			210.9	291.2
H_2	6.3	8.0	8.0	9.8	35.6	34.9	3.6	4.4
H_2O	270.4	277.4	435.6	441.1	932.0	965.1	282.0	287.2
N_2							344.4	348.5
NO							8.7	
O	3.8		2.4		1.1		1.6	
O_2	14.0		11.5		2.5		10.6	
OH	29.9		29.2		27.5		18.0	
Other	0.9	0.1	0.8	0.0	1.3	0.0	0.4	0.0

Table 10 LSA results of open-cycle engines assuming frozen flow at the throat and shifting equilibrium to the nozzle exit plane

Species	Emission indices (g exhaust/kg propellant)							
	LOX/RP-1 GG		LOX/LCH4 GG		LOX/LH2 GG		N2O4/UDMH GG	
	Throat	Equil	Throat	Equil	Throat	Equil	Throat	Equil
BC	34.7	34.7	10.7	10.7			7.9	7.9
CH4	12.7	12.7	35.0	35.0			4.8	4.8
CO	318.1	256.8	212.2	159.5			128.4	85.5
CO_2	313.7	410.1	268.0	350.9			193.9	261.3
H_2	9.1	9.5	9.7	10.1	37.8	34.3	6.9	7.6
H_2O	256.2	275.6	415.1	433.5	895.1	965.3	274.5	280.0
N_2							349.3	352.8
NO							7.3	
O	4.6		3.0		3.5		1.4	
O_2	18.3		14.6		12.3		8.3	
OH	31.7	0.6	30.9	0.2	49.8	0.4	16.7	
Other	0.9	0.0	0.8	0.1	1.5	0.0	0.6	0.1

the regenerative cooling efficiency, a variation of the film cooling share is of interest. In this parametric variation, the share is both halved and doubled from the nominal of 3%. Figure 13 and Table 12 show the results of this analysis. A higher share of film cooling leads to a higher fraction of BC and CH_4 in the exhaust. For the LOX/RP-1 GG engine, a share of 6% leads to a total BC content of almost 50 g in the exhaust per kilogram propellant, an increase of about 11.4 g/kg compared to the low 1.5% version. Overall, the impact is lower for the propellant combination LOX/LCH4 than for LOX/RP-1.

4 Discussion

The primary goal of this study was to establish a reference dataset detailing rocket engine exhaust distributions (primary emission indices) for use in launch emission inventories in the absence of detailed, proprietary rocket engine models. Because the baseline ENTRAIN rocket engines are uniformly designed for a 2200 kN thrust class, they provide a consistent comparative baseline. To accurately reflect the realities of contemporary launch vehicles, a set of N2O4/UDMH hypergolic engines and an ammonium perchlorate/aluminum/HTPB solid rocket motor of the same thrust class were integrated into the analysis.

Each engine was modeled with RPA, incorporating a simplified cycle analyses for the liquid propellant engines. A validation comparing the RPA equilibrium combustion processes against standard CEA models demonstrated very good agreement.

The reference engine exhaust profiles are detailed across all engine and cycle combinations. Because closed-cycle engines combust all of their propellant in the main combustion chamber, their resulting exhaust products are comparatively the "cleanest". In contrast, gas generators operate at highly fuel-rich O/F ratios, consequently expelling significant quantities of partially combusted propellant. This

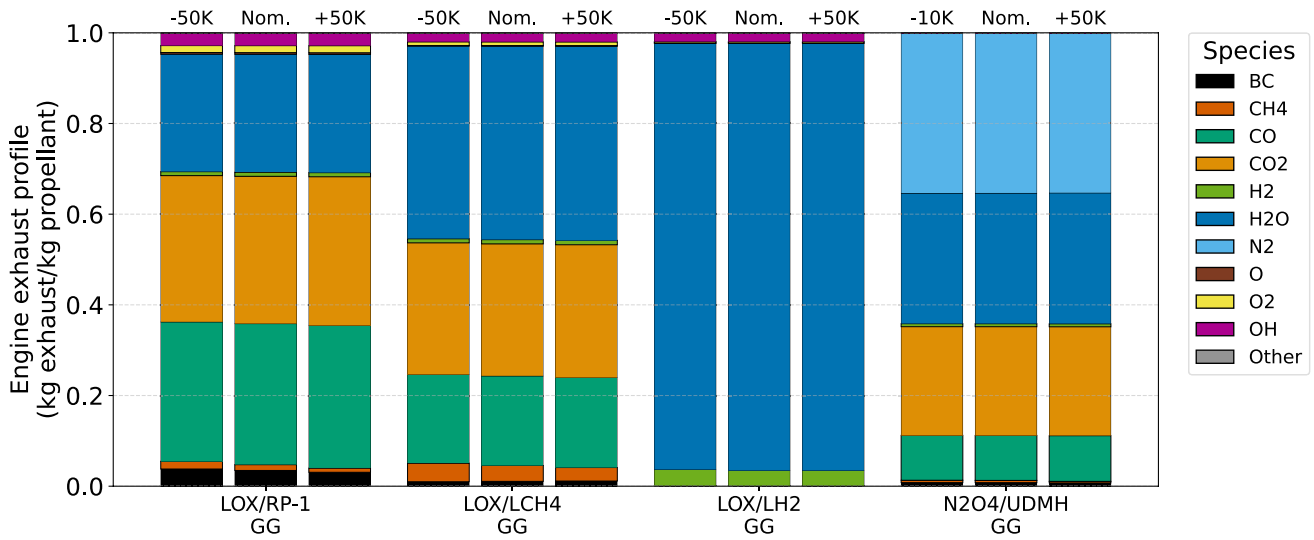

Fig. 12 LSA open-cycle engine exhaust profiles for GG temperature variation

Table 11 LSA results of open-cycle engines for GG temperature variation

Species	Emission indices (g exhaust/kg propellant)							
	LOX/RP-1 GG		LOX/LCH4 GG		LOX/LH2 GG		N2O4/UDMH GG	
	−50 K	+50 K	−50 K	+50 K	−50 K	+50 K	−10 K	+50 K
BC	37.9	30.7	9.8	11.4			8.0	7.3
CH4	16.9	9.1	40.9	29.7			5.1	3.4
CO	307.2	315.1	196.1	198.4			99.0	100.7
CO_2	322.9	327.7	289.9	293.0			239.7	240.2
H_2	8.7	9.1	8.9	9.7	36.5	34.0	6.6	6.6
H_2O	259.1	260.8	425.0	428.2	940.6	943.0	287.8	288.5
N_2							352.8	352.3
NO							0.1	0.1
O	3.7	3.7	1.4	1.4	0.7	0.7		
O_2	15.3	15.5	7.9	7.9	3.0	3.0		
OH	27.4	27.7	19.6	19.7	18.5	18.5	0.7	0.7
Other	0.9	0.6	0.5	0.6	0.7	0.8	0.2	0.2

disparity is clearly illustrated in the diagrams separating the main chamber and gas generator exhaust streams. For example, the LOX/RP-1 GG engine expels approximately three times as much BC as the LOX/LCH4 variant, whereas the LOX/LCH4 GG engine emits roughly three times as much unburnt methane. These elevated BC shares in the LOX/RP-1 exhaust are a direct physical result of the higher carbon-to-hydrogen ratio inherent to RP-1 compared to methane.

The local sensitivity study shows that even small variations in the model parameters can lead to measurable changes in the exhaust composition. The O/F ratio and the frozen area ratio are critical for the dominant exhaust products coming out of the main combustion chamber. For hydrocarbon engines, these parameters clearly have an impact on the overall distribution of CO, CO_2, and H_2O as the three primary exhaust products.

In contrast, the gas generator temperature (or its O/F ratio) and the share of film cooling has a much larger impact on BC and CH_4 in the exhaust of the hydrocarbon and hypergolic engines.

4.1 Black carbon

A further general remark concerns the treatment of BC in existing inventories. Literature estimates for BC are

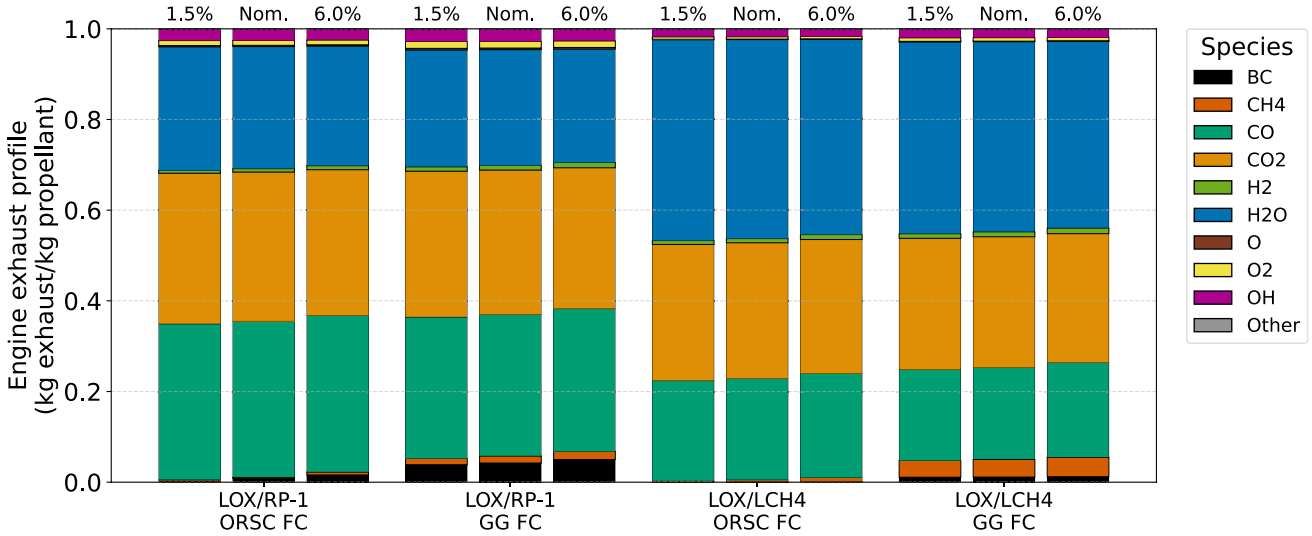

Fig. 13 LSA engine exhaust profiles for film cooling variations

Table 12 LSA results of engines for film cooling variations

Species	Emission indices (g exhaust/kg propellant)							
	LOX/RP-1 ORSC FC		LOX/RP-1 GG FC		LOX/LCH4 ORSC FC		LOX/LCH4 GG FC	
	1.5%	6.0%	1.5%	6.0%	1.5%	6.0%	1.5%	6.0%
BC	4.0	16.0	38.5	49.9	0.3	1.2	11.0	12.0
CH4	1.6	6.3	14.0	18.2	2.3	9.0	37.0	43.0
CO	343.4	345.4	311.6	314.3	221.0	229.5	200.0	208.4
CO_2	332.5	321.4	321.8	311.1	300.9	295.6	289.8	284.7
H_2	6.8	8.8	9.6	11.6	8.5	10.9	10.1	12.5
H_2O	271.9	264.0	257.7	250.4	443.0	430.8	423.0	411.6
O	2.9	2.7	3.6	3.5	1.0	1.0	1.4	1.3
O_2	11.1	10.6	15.1	14.4	5.4	5.2	7.8	7.4
OH	25.1	24.0	27.2	25.9	17.2	16.4	19.4	18.5
Other	0.7	0.8	0.9	0.7	0.4	0.4	0.5	0.6

predominantly derived from legacy measurements of an Atlas II launch vehicle, which utilized a LOX/RP-1 gas generator engine in its first stage [8, 30–32]. In those studies, the primary exhaust at the nozzle exit, prior to any post-combustion, was estimated at 25 g BC per kg of propellant. This specific value has subsequently been adopted by inventories, such as CSVEM and the LEAT database.

For LOX/LCH4 engines, the derivation of BC is even more indirect. In the absence of rocket-specific empirical measurements, automotive engine exhaust data has frequently been used as a proxy. Based on the observations that methane-fueled automotive engines emit approximately 80% less BC than gasoline engines, it has been widely assumed that methane rocket engines produce about 5 g BC per kg of propellant [33]. While these extrapolations may be appropriate in the absence of experimental data, their limitations are substantial. For instance, the Atlas II gas generator engine inherently produces a higher share of unburnt hydrocarbons compared with closed-cycle engines. Extrapolating these legacy results across different engine cycles and propellant combinations introduces significant errors.

Equilibrium-based combustion tools, such as CEA or RPA, do not explicitly predict BC formation. However, under significantly fuel-rich conditions (i.e., low O/F ratios), these models yield condensed carbon in the form of graphite, C(gr). In reality, combustion chamber conditions do not achieve ideal chemical equilibrium, especially not in gas generators. Finite-rate kinetics, turbulent mixing, and rapid expansion are more likely to produce complex, partially oxidized hydrocarbon species that act as soot precursors rather

than pure graphite. Nevertheless, from a thermodynamic standpoint, the formation of condensed carbon in equilibrium calculations can serve as a first-order estimate for potential BC formation when more sophisticated combustion models are unavailable. For example, Fig. 14 demonstrates that the C(gr) exhaust for the LOX/RP-1 GG ENTRAIN engine is on the same order of magnitude as the Atlas II-derived BC estimates (3.5% standard model or 4.2% incl. film cooling vs. 2.5% Atlas II).

Beyond the prediction of BC in the combustion products of the gas generator, it is unclear how the BC could potentially change its state or particle size when being expanded in the turbine and subsequent nozzle.

4.2 Comparison to existing datasets

Because this study aims to establish a new reference for primary rocket engine exhaust that includes the influence of turbopump cycles, the results must be benchmarked against the existing emission profiles identified in chapter 2. While generalized reference datasets are highly valuable in the absence of detailed data, the ultimate goal of all emission inventories should be the individual modeling of specific engines.

Before analyzing individual propellant combinations, several general methodological considerations must be addressed. The inventories considered herein (Ross, Pradon, Barker and Brown) state that their exhaust profiles do not account for chemical changes occurring after the exhaust gas leaves the nozzle. Because rockets carry both fuel and oxidizer on board, the fundamental principle of mass conservation dictates that the total primary exhaust mass cannot exceed the initial propellant mass. However, this constraint is violated in several published results.

Even when inventories correctly enforce mass conservation by employing rigorous chemical equilibrium codes, they frequently oversimplify the physical engine architecture. Generally, because CSVEM and LEAT at 120 km databases utilize CEA methods, their distributions for all liquid propellant combinations closely align with the closed-cycle engines modeled in this study. Notably, none of the existing inventories account for the separate mass flows generated by secondary streams, such as the gas generator exhaust.

4.2.1 LOX/RP-1

Figure 14 plots the propellant combination LOX/RP-1. The datasets from Ross, Pradon, Barker, and Brown differ considerably from the reference datasets established in this study. Ross, Pradon, and Brown assume ideal stoichiometric combustion, resulting in an exhaust composed entirely of CO_2 and H_2O. Additionally, the datasets from Pradon and Barker significantly exceed the 1 kg exhaust per 1 kg propellant threshold.

4.2.2 LOX/LCH4

A greater degree of consensus is observed for LOX/LCH4, as shown in Fig. 15. None of the exhaust profiles exceed the mass conservation limit beyond the explicit addition of BC in certain inventories. With the exception of the stoichiometric LEAT dataset, all inventories feature a similar distribution of CO, CO_2, and H_2O. The variance in the specific mass fractions most likely stems from differences in assumed engine O/F ratios and equilibrium assumptions through the nozzle. In this study, the ENTRAIN models freeze the equilibrium flow at a specific area ratio downstream of the throat (1.8 for LOX/LCH4). This may not be the case for the other models, as CEA restricts users to freezing the flow exactly

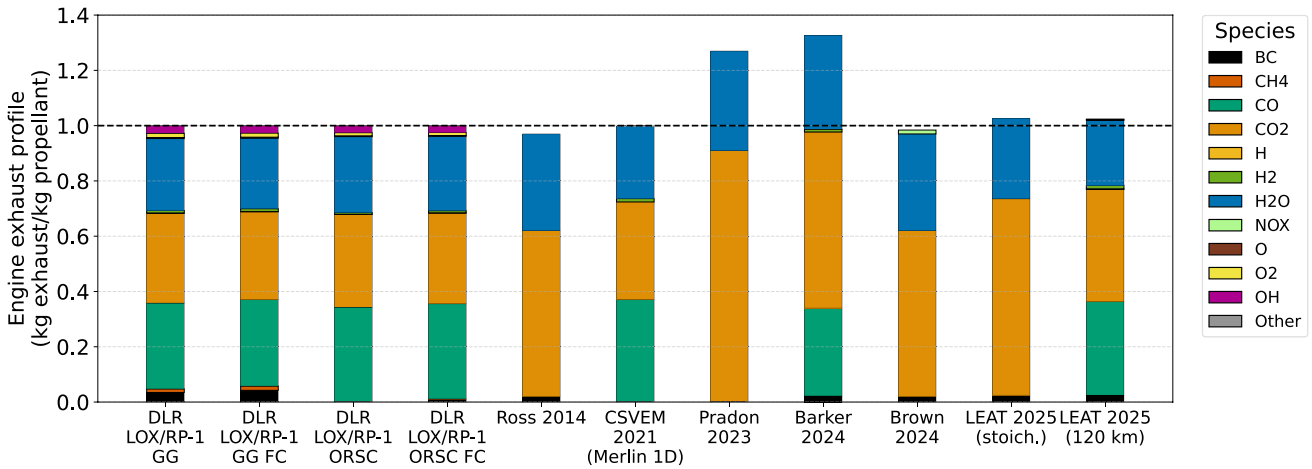

Fig. 14 Comparison of reference LOX/RP-1 engines to existing inventories/exhaust definitions [4–9]

at the throat or maintaining equilibrium through to the nozzle exit. Both of these conditions are considered extreme as one might be too conservative while the other might be too optimistic. The lower CO values in the Barker and LEAT at 120 km datasets indicate that equilibrium flow was assumed throughout the entire nozzle, affording the flow more time for chemical reactions.

4.2.3 LOX/LH2

The LOX/LH2 comparison shown in Fig. 16 reveals a situation similar to LOX/RP-1. Ross, Pradon, and Brown assume stoichiometric combustion, yielding only water in the exhaust. Once again, the datasets from Pradon and Barker exceed the total initial propellant mass.

4.2.4 N2O4/UDMH

Figure 17 provides an overview of the hypergolic propellant combination N2O4/UDMH. It is notable that the cumulative exhaust masses reported by Ross, Pradon, Barker, and Brown are substantially below 1 kg exhaust per kg propellant. This is likely because the N_2 exhaust was omitted from the emission tables due to its abundant natural presence in the atmosphere. Ross, Pradon, and Brown assume stoichiometric combustion. It should also be noted that the Ross dataset utilized N2O4/N2H4 rather than N2O4/UDMH, leading to a different stoichiometric baseline.

4.2.5 Solid rocket motors

The comparison of solid rocket motors is illustrated in Fig. 18. While CSVEM and LEAT at 120 km again have

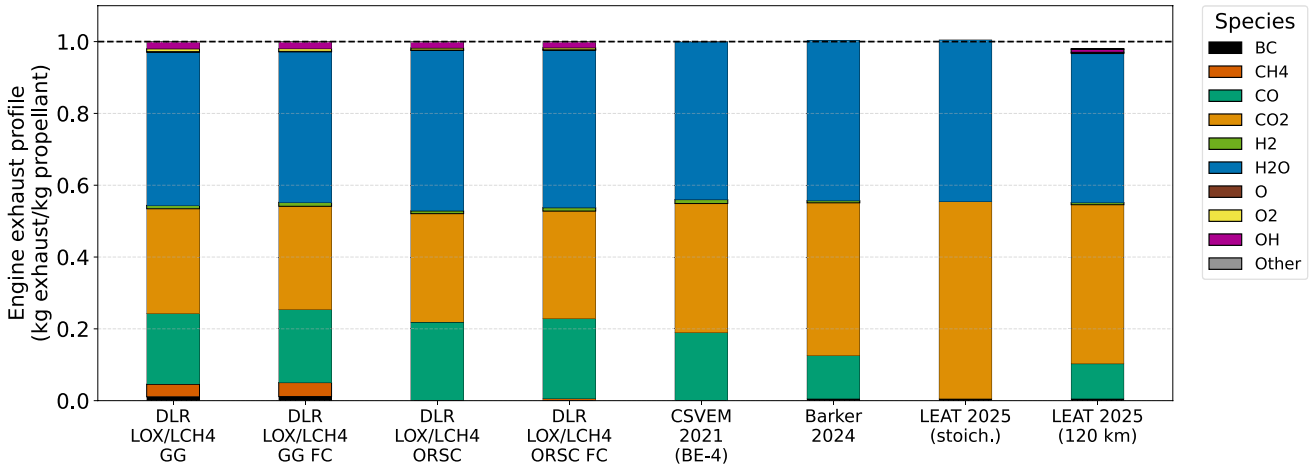

Fig. 15 Comparison of reference LOX/LCH4 engines to existing inventories/exhaust definitions [6, 8, 9]

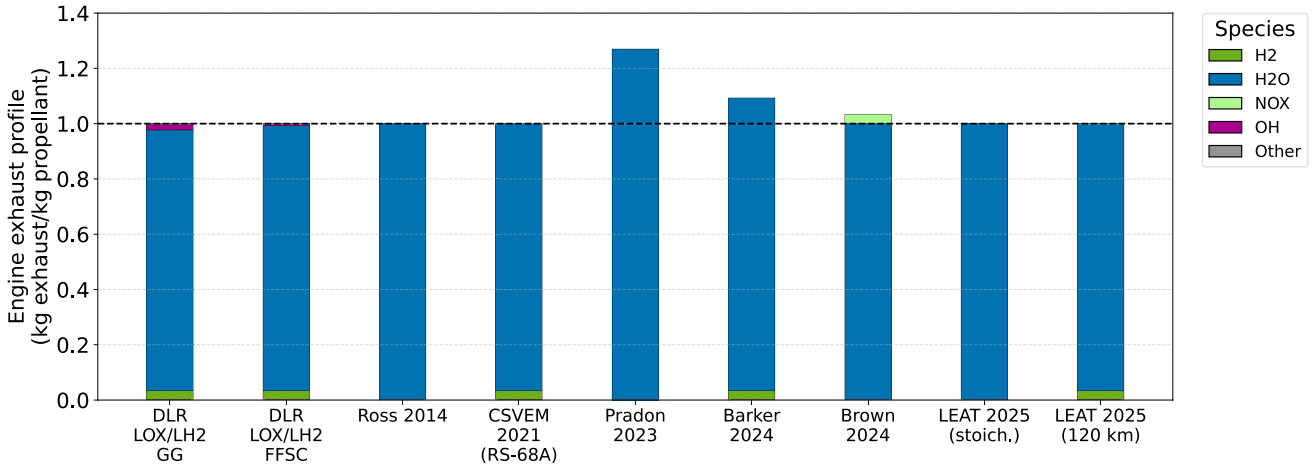

Fig. 16 Comparison of reference LOX/LH2 engines to existing inventories/exhaust definitions [4–9]

similar distributions due to their shared use of CEA, the LEAT dataset prominently features elemental Cl in the exhaust. The cumulative exhaust masses from Pradon, Barker, Brown, and the stoichiometric LEAT are significantly above the 1 kg limit. Across all datasets, there is a large variance in the predicted exhaust species and their relative distributions. Similar to the N2O4/UDMH case, it is likely that Ross, Pradon, Barker, and Brown excluded N_2 from their final mass totals.

The CEA-based datasets generally consist of approximately one-third Al_2O_3, one-third CO, and a remaining third comprising N_2, HCl, H_2O, and H_2. In contrast, the Ross distribution accounts only for Al_2O_3, BC, CO_2, and H_2O. The Pradon, Barker, and stoichiometric LEAT distributions add HCl to the list. Brown reports "Alumina" rather than specific Al_2O_3 emission indices and includes a large share of "reactive chlorine", while Barker reports a substantial fraction of pure Cl and Cl_2.

4.2.6 Summary of comparisons

Finally, comparing the exhaust profiles generated in this study with existing datasets reveals methodological discrepancies. First, there is a fundamental divergence between datasets that apply CEA methods at realistic O/F ratios versus those that assume ideal stoichiometric combustion.

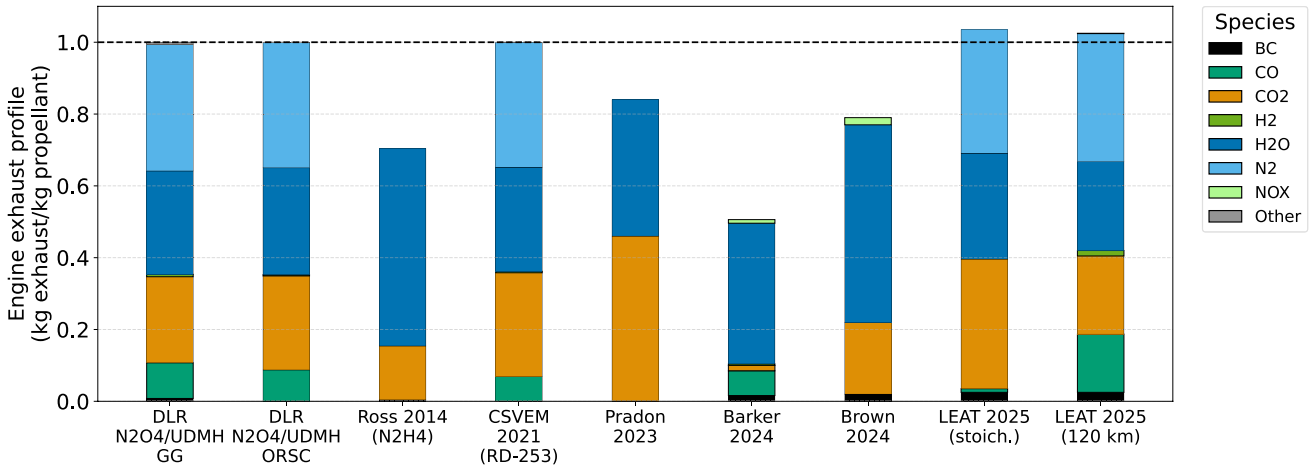

Fig. 17 Comparison of reference N2O4/UDMH engines to existing inventories/exhaust definitions [4–9]

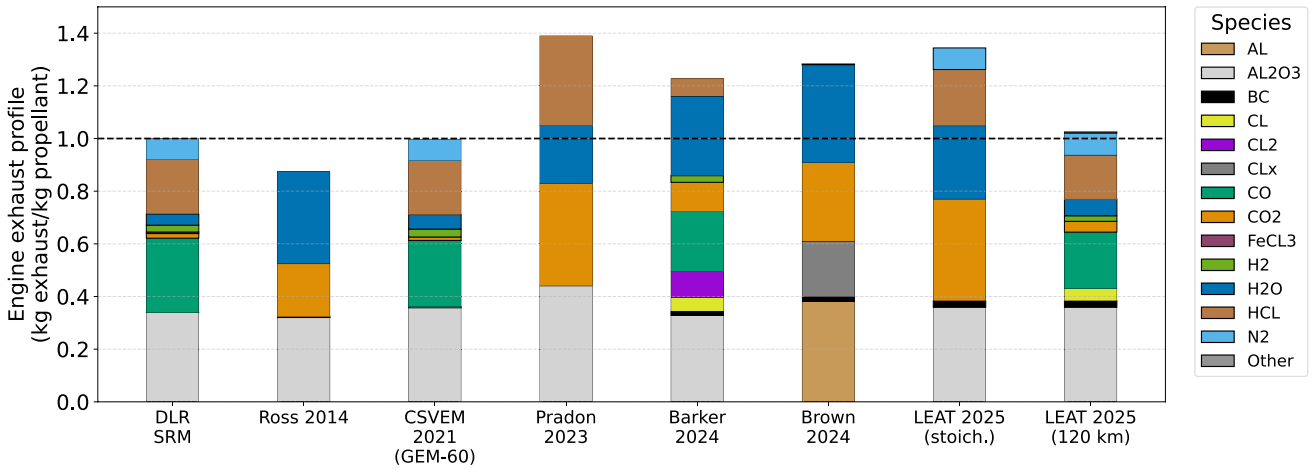

Fig. 18 Comparison of reference solid propellant engines to existing inventories/exhaust definitions [4–9]

Second, by explicitly modeling the separate mass flows inherent to the gas generator engine cycle, this study produces a significantly different overall exhaust distribution. The isolated gas generator exhaust stream contains a high concentration of carbon and other notable species, such as pure methane. In contrast, existing inventories typically extrapolate BC emissions based primarily on legacy measurement data from the Atlas II launch vehicle, which fails to capture the influence of engine turbopump cycles.

4.3 Limitations

A fundamental limitation of this study is the reliance on 0D equilibrium codes, which inherently neglect the complex finite-rate reaction kinetics occurring within the combustion chamber. This simplification is particularly critical when determining combustion products from the non-equilibrium conditions typical of a gas generator, resulting in lower GG temperatures than predicted with equilibrium methods. While high-fidelity computational fluid dynamics could address these non-equilibrium effects, such models are computationally expensive and still struggle to accurately resolve detailed chemical kinetics, making them impractical for establishing reference datasets.

Important exhaust byproducts, such as BC and soot, are primarily formed under these non-equilibrium conditions [34]. However, because equilibrium codes condense these elements into solid carbon in its lowest energy form, this output can effectively serve as a first-order estimate for BC. Furthermore, because this study strictly considers exhaust properties up to the nozzle exit plane, the data cannot be used as a direct input for climate modeling without accounting for the plume mixing with the atmosphere.

Another major limitation of 0D equilibrium programs is the assumption of perfectly homogeneous combustion. To address this, an exploratory study investigated the implementation of fuel film cooling using a simplified thermodynamics approach. By assuming that 3% of the total mass flow operates at a distinct, highly fuel-rich O/F ratio, the results indicate the introduction of a measurable fraction of solid carbon into the exhaust. Similar to the gas generator findings, this carbon-adding effect is more pronounced for LOX/RP-1 than for LOX/LCH4. By accounting for film cooling, even closed-cycle hydrocarbon engines demonstrate a measurable carbon output, which aligns with visual observations of real-world exhaust plumes from such engines. However, given the broad assumptions and inherent limitations of this simplified 0D exploratory study, these specific quantitative results should be interpreted with caution.

The assumption of perfectly homogeneous combustion also presents limitations in the case of solid rocket motors. Although experimental studies confirm the presence of soot or BC in the exhaust [35], these solid particulates are not predicted in our reference dataset. Because 0D equilibrium codes only evaluate the global bulk mixture, they cannot capture the highly complex, localized effects such as diffusional mixing [36]. Accurately predicting the BC formation would require far more sophisticated models.

5 Conclusion

Characterizing primary rocket engine exhaust compositions is a critical prerequisite for accurately assessing the radiative forcing impacts of launch vehicle atmospheric emissions. This study provides a comprehensive reference dataset of engine exhaust modeled up to the nozzle exit plane, that is designed for integration into global launch inventories when detailed engine models are unavailable.

This dataset builds upon generic engine concepts from the ENTRAIN RLV study, expanded to include a hypergolic propellant combination and a typical modern solid rocket motor to better reflect current global launch architectures. Nominal exhaust distributions are detailed for all evaluated engines, with a particular emphasis placed on isolating the separate exhaust streams characteristic of gas generator cycles. Additionally, an exploratory study utilizing a simplified approach to analyze the effects of film cooling demonstrated that this modeling approach leads to the expected higher carbon levels into the exhaust of hydrocarbon-fueled engines. The reference datasets were supported with targeted parametric variations to assess the uncertainty associated with some of the modeling parameters.

A comparison between these newly established reference datasets and existing inventories highlights that exhaust distributions can vary significantly depending on the underlying methodological assumptions. By utilizing a consistent, thrust-normalized methodology, incorporating diverse rocket engine cycle types, and exploring the impacts of film cooling, this study establishes robust reference rocket engine exhaust datasets to improve the baseline fidelity of launcher inventories used in atmospheric and climate modeling.

Ideally, the assessment of each specific launch vehicle in global launch inventories would be based on bespoke engine analysis to account for the heterogeneity in rocket engine designs or exact solid propellant formulations. However, in the absence of engine-specific models or sufficient data to generate them, this study offers a robust baseline based on thermodynamic and engine-cycle principles.

Future work should focus on increasing the model fidelity in cases where the equilibrium methods reach their limits, and on the uncertainty quantification of the global model beyond the local sensitivity analysis performed herein.

Given the physical and chemical gap between the exhaust at the nozzle exit plane (or primary emissions) and the fully

post-combusted products required by climate models, additional numerical and experimental efforts are required to better characterize the plume mixing and dispersion. To apply these models to entire launcher inventories without excessive computational cost, fast and sufficiently accurate engineering approaches are needed.

Ultimately, the engine exhaust distributions presented in this study provide a consistent reference dataset for the scientific community, encompassing all relevant modern launcher propellant combinations and engine turbopump cycles.

Appendix

Reference dataset including all trace gases

All values are rounded to 3 decimals.

Species	Emission indices (g exhaust/kg propellant)								
	LOX/RP-1 ORSC	LOX/RP-1 GG	LOX/LCH4 ORSC	LOX/LCH4 GG	LOX/LH2 FFSC	LOX/LH2 GG	N2O4/ UDMH ORSC	N2O4/ UDMH GG	Solid rocket motor
AlH_2O_2Cl									0.004
Al_2O_3									339.658
AlCl									0.011
$AlCl_2$									0.002
$AlCl_3$									0.043
AlOH									0.002
AlOHCl									0.001
$AlOHCl_2$									0.054
BC		34.731		10.662				7.921	
C_2H_6				0.002					
CH_4		12.665		35.032				4.843	
CO	342.734	310.721	218.209	197.240			87.200	99.222	281.417
CO_2	336.146	325.353	302.621	291.542			262.059	239.769	17.507
COOH	0.019	0.015	0.007	0.006					
Cl									0.436
Cl_2									0.001
$FeCl_3$									5.902
H	0.679	0.687	0.437	0.461	0.394	0.670	0.034	0.032	0.038
H_2	6.151	8.952	7.638	9.300	34.799	35.190	3.146	6.607	26.004
H_2O	274.530	260.159	447.015	426.749	959.427	941.901	297.749	287.947	42.516
H_2O_2	0.008	0.008	0.005	0.005		0.002			
HCHO	0.001								
HCN									0.001
HCO	0.014	0.010	0.004	0.003					
HCOOH	0.003	0.002	0.002	0.001					
HCl									205.655
HO_2	0.044	0.051	0.017	0.020	0.001	0.007			
N_2							348.399	352.725	80.734
NH_3								0.020	0.001
NO							0.235	0.134	
O	2.903	3.699	1.060	1.433	0.065	0.697	0.013	0.007	
O_2	11.253	15.368	5.486	7.886	0.162	3.017	0.115	0.049	
OH	25.516	27.579	17.499	19.66	5.152	18.515	1.050	0.725	0.014

Author contributions S.C. conducted the primary investigation, performed the data analysis, and wrote the original draft of the manuscript. M.H., J.W., and M.S. contributed to the conceptualization and methodology of the study. M.S. developed and provided the original ENTRAIN engine models utilized in this research. J.W. contributed to the drafting of the literature and methodology sections. J.W. and M.S. reviewed and edited the final manuscript.

Funding Open Access funding enabled and organized by Projekt DEAL. This work was performed within the DLR internal initiative S3D + and the DLR project S3D-BETTER.

Data availability No datasets were generated or analyzed during the current study.

Declarations

Conflict of interest The authors have no relevant financial or non-financial interests to disclose.

Open Access This article is licensed under a Creative Commons Attribution 4.0 International License, which permits use, sharing, adaptation, distribution and reproduction in any medium or format, as long as you give appropriate credit to the original author(s) and the source, provide a link to the Creative Commons licence, and indicate if changes were made. The images or other third party material in this article are included in the article's Creative Commons licence, unless indicated otherwise in a credit line to the material. If material is not included in the article's Creative Commons licence and your intended use is not permitted by statutory regulation or exceeds the permitted use, you will need to obtain permission directly from the copyright holder. To view a copy of this licence, visit http://creativecommons.org/licenses/by/4.0/.

References

1. IPCC.: Climate Change 2023: Synthesis report. Contribution of working groups I, II and III to the sixth assessment report for the intergovernmental panel on climate change [Core Writing Team, H. Lee and J. Romero (eds.)]. IPCC, Geneva, Switzerland. (2023) https://doi.org/10.59327/IPCC/AR6-9789291691647
2. Lee, D.S., Fahey, D.W., Skowron, A., et al.: The contribution of global aviation to anthropogenic climate forcing for 2000 to 2018. Atmos. Environ. (2021). https://doi.org/10.1016/j.atmosenv.2020.117834
3. Ryan, R.G., Marais, E.A., Balhatchet, C.J., Eastham, S.D.: Impact of rocket launch and space debris air pollutant emissions on stratospheric ozone and global climate. Earths Future (2022). https://doi.org/10.1029/2021EF002612
4. Ross, M.N., Sheaffer, P.M.: Radiative forcing caused by rocket engine emissions. Earth's Future **2**(4), 177–196 (2014). https://doi.org/10.1002/2013EF000160
5. Pradon, C.V.M., Eastham, S.D., Chossière, G., et al.: Global three-dimensional emission inventory for launch vehicles from 2009 to 2018. J. Spacecr. Rockets **60**(3), 716–727 (2023). https://doi.org/10.2514/1.A35385
6. Barker, C.R., Marais, E.A., McDowell, J.C.: Global 3D rocket launch and re-entry air pollutant and CO_2 emissions at the onset of the megaconstellation era. Sci. Data (2024). https://doi.org/10.1038/s41597-024-03910-z
7. Brown, T.F.M., Bannister, M.T., Revell, L.E., et al.: Worldwide rocket launch emissions 2019: an inventory for use in global models. Earth Space Sci. (2024). https://doi.org/10.1029/2024EA003668
8. National Academies of Sciences, Engineering and Medicine: Commercial Space Vehicle Emissions Modelling. The National Academies Press, Washington, DC (2021). https://doi.org/10.17226/26142
9. Fischer, J. S., Winterhoff, S., Fasoulas, S.: Launch emission assessment tool (LEAT). University of Stuttgart. https://github.com/lcasts/LEAT (2025) Accessed Feb 2026
10. Herberhold, M., Wilken, J., Callsen, S., Sippel, M.: DLR global launch emission inventory 2024: overview and initial results. 76th International Astronautical Congress (IAC), Sydney, Australia (2025)
11. European Space Agency (ESA LCA WG): Space system life cycle assessment (LCA) Guidelines. ESSB-HB-U-005, Issue 2 Rev. 0. https://esamultimedia.esa.int/docs/spacesafety/Space_System_Life_Cycle_Assessment_Guidelines.pdf (2025) Accessed Feb 2026
12. Dietlein, I., Bussler, L., Stappert, S., et al.: Overview of system study on recovery methods for reusable first stages of future European launchers. CEAS Space J. **17**, 71–88 (2025). https://doi.org/10.1007/s12567-024-00557-9
13. Sippel, M., Wilken, J.: Selection of propulsion characteristics for systematic assessment of future European RLV-options. CEAS Space J. **17**, 89–111 (2025). https://doi.org/10.1007/s12567-024-00564-w
14. NPO Energomash: RD-253. Retrieved from: https://web.archive.org/web/20150405185423/http://www.npoenergomash.ru/eng/dejatelnost/engines/rd253/ Accessed Feb 2026
15. Astronautix: RD-275. http://www.astronautix.com/r/rd-275.html Accessed Feb 2026
16. Astronautix: RD-250. http://www.astronautix.com/r/rd-250.html Accessed Feb 2026
17. Sutton, G.P., Biblarz, O.: Rocket Propulsion Elements, Ninth Edition John Wiley & Sons, Inc, Hoboken, New Jersey, USA (2017)
18. Maggi, F., Dossi, S., Paravan, C.: Detailed properties of iron oxide solid propellant catalyst. 7th European Conference for Aeronautics and Space Sciences (EUCASS), Milan, Italy (2017). https://doi.org/10.13009/EUCASS2017-674
19. Rocket Propulsion Software+Engineering UG: Rocket Propulsion Analysis (RPA), Version 2.3.2. https://www.rocket-propulsion.com/ (2017) Accessed Feb 2026
20. Ponomarenko, A.: RPA: Tool for Liquid propellant rocket engine analysis C++ implementation.. https://www.rocket-propulsion.com/downloads/pub/RPA_LiquidRocketEngineAnalysis_II.pdf (2010) Accessed Feb 2026
21. Gordon, S., McBride, B.J.: Computer program for calculation of complex chemical equilibrium compositions and applications, Part I: Analysis. NASA RP-1311 (1994)
22. Glassman, I., Yetter, R.A.: Combustion, Fourth Edition Academic Press (2008)
23. van Schyndel, J., Goos, E., Naumann, C., et al.: Effects of compounds in liquefied methane on rocket engine operation. Aerospace **9**, 698 (2022). https://doi.org/10.3390/aerospace9110698
24. U.S. Department of defense: detail specification propellant, rocket grade kerosene, MIL-DTL-25576F (2023)
25. Nickerson, G.R., Dang, L.D., Coats, D.E.: Engineering and programming manual: two-dimensional kinetic reference computer program (TDK). NASA CR 178628, software and engineering associates, Inc, Carson City, NV, United States (1985)
26. Pieper, J.L., Dean, L.E., Valentine, R.S.: Mixture ratio distribution–its impact on rocket thrust chamber performance. J. Spacecr. **4**, 6 (1967). https://doi.org/10.2514/3.28952
27. Shine, S.R., Shri Nidhi, S.: Review on film cooling of liquid rocket engines. Propuls. Power Res. **7**(1), 1–18 (2018). https://doi.org/10.1016/j.jppr.2018.01.004

28. Yang, V., Anderson, W.E.: Liquid Rocket Engine Combustion Stability. American Institute of Aeronautics and Astronautics (1995)
29. Ponomarenko, A.: RPA: Tool for rocket propulsion analysis. assessment of delivered performance of thrust chamber. Available at: https://www.rocket-propulsion.com/downloads/pub/RPA_AssessmentOfDeliveredPerformance.pdf (2013) Accessed Jun 2026
30. Simmons, F.S.: Rocket Exhaust Plume Phenomenology. The Aerospace Press, California, USA (2000)
31. Plastinin, Y. Karabadzhak, G.F., Khmelinin, B. et al.: Investigation of soot density in the LOX/kerosene engine booster exhaust of Atlas II and Atlas III from remote measurements of radiation intensity. 43rd AIAA Aerospace Sciences Meeting and Exhibit, Nevada, USA (2005). https://doi.org/10.2514/6.2005-769
32. Alexeenko, A.A., Gimelshein, N.E., Levin, D.A., et al.: Modeling of flow and radiation in the Atlas plume. J. Thermophys. Heat Transf. (2002). https://doi.org/10.2514/2.6651
33. Wang, Y., Xing, Z., Xu, H., Du, K.: Emission factors of air pollutants from CNG-gasoline bi-fuel vehicles: Part I. Black carbon. Sci. Total. Environ. **572**, 1161–1165 (2016). https://doi.org/10.1016/j.scitotenv.2016.08.027
34. Yu, J., Lee, C.: Prediction of non-equilibrium kinetics of fuel-rich kerosene/LOX combustion in gas generator. J. Mech. Sci. Technol. **21**, 1271–1283 (2007). https://doi.org/10.1007/BF03179044
35. Decker, T. G., Rialland, V., Langenais, A.: Infrared radiation from soot particles in rocket engine plume: comparison between numerical simulations and propulsion bench experiments. 25th joint ONERA-DLR Aerospace Symposium (2025)
36. Beckstead, M.W., Derr, R.L., Price, C.F.: A model of composite solid-propellant combustion based on multiple flames. AIAA J. (1970). https://doi.org/10.2514/3.6087

Publisher's Note Springer Nature remains neutral with regard to jurisdictional claims in published maps and institutional affiliations.